nature communications

Article

https://doi.org/10.1038/s41467-024-55295-7

# Selectively targeting the AdipoR2-CaM-CaMKII-NOS3 axis by SCM-198 as a rapid-acting therapy for advanced acute liver failure

Received: 13 April 2024

Accepted: 8 December 2024

Published online: 16 December 2024

Check for updates

Rui Wang[1,5], Youwei Chen[1,2,5], Jiazhen Han[1], Huikang Ye[1], Huiran Yang[1], Qianyan Li[1], Yizhen He[1], Boyu Ma[3], Junjie Zhang[3], Yanli Ge[3], Zhe Wang[3], Bo Sun[3], Huahua Liu[1], Liming Cheng[1,4] ✉, Zhirong Wang[3] ✉ & Gufa Lin[1,2] ✉

Acute liver failure (ALF) is a hepatology emergency with rapid hepatic destruction, multiple organ failures, and high mortality. Despite decades of research, established ALF has minimal therapeutic options. Here, we report that the small bioactive compound SCM-198 increases the survival of male ALF mice to 100%, even administered 24 hours after ALF establishment. We identify adiponectin receptor 2 (AdipoR2) as a selective target of SCM-198, with the AdipoR2 R335 residue being critical for the binding and signaling of SCM-198-AdipoR2 and AdipoR2 Y274 residue serving as a molecular switch for $Ca^{2+}$ influx. SCM-198-AdipoR2 binding causes $Ca^{2+}$ influx and elevates the phosphorylation levels of CaMKII and NOS3 in the AdipoR2-CaM-CaMKII-NOS3 complex identified in this study, rapidly inducing nitric oxide production for liver protection in murine ALF. SCM-198 also protects human ESC-derived liver organoids from APAP/TAA injuries. Thus, selectively targeting the AdipoR2-CaM-CaMKII-NOS3 axis by SCM-198 is a rapid-acting therapeutic strategy for advanced ALF.

Acute liver failure (ALF) is a hepatology emergency with rapid hepatic destruction, multiple organ failures, and high (~30%) mortality[1–5]. Despite decades of research, established ALF has minimal therapeutic options, frequently necessitating liver transplantation as the last recourse[1–5].

ALF can be caused by various etiologies, including drug overdose, systemic infections and inflammations, and autoimmune diseases[1–3]. Excessive use of anti-infectious or analgesic drugs represents a common cause of chemically-induced ALF. Paracetamol (APAP), for instance, is a prominent contributor to ALF-related fatalities in both the United States and China[1–7]. APAP-induced hepatotoxicity is driven by its intermediate metabolite, N-acetyl-p-benzoquinone imine (NAPQI), a highly reactive substance that binds covalently to the sulfhydryl groups in cellular and mitochondrial proteins. The binding triggers a cascade of mitochondrial oxidative stress and dysfunction, culminating in hepatocyte necrosis[8–10]. The necrotic cells release inflammatory mediators like TNF-α and HMGB1, fueling uncontrolled sterile inflammation and extensive hepatocyte death[1–5,9], which cause systemic inflammatory response syndrome (SIRS), a hallmark of ALF[1–5]. In human patients, ALF may ensue soon after APAP intoxication, with

[1]Key Laboratory of Spine and Spinal Cord Injury Repair and Regeneration of Ministry of Education, Department of Orthopedic, Tongji Hospital affiliated to Tongji University, School of Life Sciences and Technology, Tongji University, Shanghai, China. [2]School of Medicine, Tongji University, Shanghai, China. [3]Department of Gastroenterology, Tongji Hospital affiliated to Tongji University, School of Medicine, Tongji University, Shanghai, China. [4]Clinical Center for Brain and Spinal Cord Research, Tongji University, Shanghai, China. [5]These authors contributed equally: Rui Wang, Youwei Chen.
✉e-mail: limingcheng@tongji.edu.cn; wangzr929@126.com; lingufa@tongji.edu.cn

alanine aminotransferase (ALT) and aspartate aminotransferase (AST) peaking around 36–48 h after intoxication[11]. ALF needs to be managed and treated timely[1–5]. For example, if initiated within the initial 4–8 h following APAP overdose, patients can be treated effectively with N-acetyl cysteine (NAC), which replenishes the glutathione (GSH) reserve essential for detoxifying NAPQI[1–3,12–18]. However, the effectiveness of NAC treatment diminishes after 8 h[13–17], as GSH levels deplete rapidly post-intoxication[19].

Many animal ALF models are used to investigate the pathology and progression of human ALF and to search for new treatments for ALF[11,20–27]. Both APAP- and thioacetamide (TAA)-induced murine ALF models resemble the progression of human liver failure and are widely used[20,27–30]. Like APAP, TAA-induced hepatotoxicity is mediated by its metabolite intermediate, the highly reactive thioacetamide S,S-dioxide ($TTAS_2$), which covalently binds to proteins and depletes the GSH pool[28]. Inflammatory ALF models generated by injection of lipopolysaccharide (LPS) and D-galactosamine (D-GalN) are also valuable for studying ALF progression and testing treatments, such as stem/progenitor cell transplantation[31–33].

Several molecules have been identified as hepatoprotective using the TAA, APAP, and LPS/D-GalN models[21,22,26]. However, these molecules all need to be administered in the very early (< 2) h after, or even before, the introduction of hepatotoxins (hence before ALF commencement). Currently, the maximum treatment window for murine ALF models remains within 2-3 h after liver intoxication[21,25]. NAC is also effective in treating murine APAP-induced ALF models when administered early. However, its protective efficacy rapidly diminishes beyond this window, dropping from 80% protection at 0.5 h post-intoxication (hpi) to less than 50% at 3 hpi. Unfortunately, a 'cure' for late ALF (for example, more than 12 hpi in murine models) has not been achieved.

The bioactive small molecule SCM-198 (CAS No.: 24697-74-3), a synthetic form of Leonurine (chemical structure shown in Supplementary Fig. S1a), has demonstrated antioxidant, anti-inflammatory, and anti-apoptotic effects in various pathological processes, including myocardial infarction and stroke[34,35]. It has been proposed as an alternative to statins for atherosclerosis treatment and has passed phase I clinical trials for safety and feasibility in treating hyperlipidemia[34–36]. However, despite years of research on SCM-198 in the neural and cardiovascular systems[34–36], its specific binding target remains undetermined, hindering its translational applications.

During our screening for compounds that protect AML12 and LX2 liver cells from oxidative stress induced by $H_2O_2$ exposure, we discovered that SCM-198 enhanced cell proliferation. This finding prompted us to investigate its potential protective effects in murine ALF models established by intraperitoneal injection of TAA (200 mg/kg), APAP (400 mg/kg), or LPS (10 μg/kg)/D-GalN (500 mg/kg), and more importantly, to search for its binding target and to decipher its molecular mechanisms, which are essential for its translational applications.

Here, we report that SCM-198 treatment exhibited a remarkable 100% survival rate in murine ALF models, whether administered at 0.5 hpi or 24 hpi when hepatotoxicity had already manifested with elevated serum ALT and AST levels[9,37]. The hepatoprotective effect of SCM-198, demonstrated by the lowered serum ALT/AST levels and attenuation of liver damage (reduced abnormal lipid accumulation/peroxidation and increased hepatocyte survival), is also rapid (within 6 h of SCM-198 administration). As ALF progression in mice is much faster than in humans[11], this finding indicates that SCM-198 can significantly extend the treatment window for ALF. On the mechanisms, we identify that the adiponectin receptor AdipoR2, but not AdipoR1, is a selective target of SCM-198. SCM-198 binds to the AdipoR2-CaM-CaMKII-NOS3 complex we discovered in liver cells. Binding of SCM-198 to AdipoR2 causes a rapid influx of $Ca^{2+}$, elevating the phosphorylation levels of CaMKII and NOS3, thereby directly activating nitric oxide (NO) synthesis, even in the presence of cycloheximide, which inhibits protein synthesis. Thus, SCM-198 selectively and directly activates the AdipoR2-CaM-CaMKII-NOS3-NO axis. Functional analysis in *Adipor2*$^{-/-}$ and *Nos3*$^{-/-}$ mice and human liver organoids further establishes that selectively and directly targeting the AdipoR2-CaM-CamKII-NOS3 axis is a rapid-acting therapeutic strategy for advanced ALF.

## Results

### SCM-198 enables full survival after ALF

We examined the therapeutic effect of SCM-198 (Supplementary Fig. S1a) on ALF in adult mice (6 ~ 8-week-old) injected with TAA (200 mg/kg) or APAP (400 mg/kg), two murine ALF models recapitulating human ALF pathophysiology[25–30]. SCM-198 (10 mg/kg), NAC (a known antidote for APAP), or saline (as untreated control) were intraperitoneally administered at 0.5 hpi (prophylactic) or 24 hpi (therapeutic). The survival of the mice was then followed to 144 hpi (Fig. 1a). While NAC increased the survival rate of mice (40% for TAA and 80% for APAP, compared to 0% and 20% in the saline group) when administered at 0.5 hpi, its hepatoprotective effect was lost when given at 24 hpi (Fig. 1b). By contrast, treatment with SCM-198 at both 0.5 hpi and 24 hpi prevented the death of ALF mice, with a survival rate of 100% (Fig. 1b).

Serum biochemical analysis in the ALF mice at 48 hpi (when most of untreated mice were still alive) showed that SCM-198 effectively reversed ALT and AST levels elevated by TAA or APAP, even when administered at 24 hpi (Fig. 1c). NAC administered at 24 hpi failed to reduce these levels (Fig. 1c). Thus, SCM-198 had better hepatoprotection compared to NAC when administered after ALF onset at 24 hpi. The effect of SCM-198 was also rapid, as manifested by the behavior of the SCM-198 treated animals (Supplementary Movie 1). Serum ALT and AST levels were significantly lowered 6 h post-treatment and further decreased 12 h after treatment (Fig.1d). These observations demonstrated that SCM-198 extends the treatment window beyond 24 h after TAA or APAP intoxication. Thus, for further analysis of the mechanisms underlying the therapeutic effect of SCM-198, hereafter, all mice were treated with SCM-198 at 24 hpi (Fig. 1a).

TAA- or APAP-induced glutathione (GSH) depletion and hepatocyte damage via oxidative stress-induced inflammation result in widespread liver necrosis[37,38]. However, SCM-198 restored GSH levels in the liver tissues (Fig. 1e) and reduced liver necrosis (Fig. 1f and Supplementary Fig. S1b–d). SCM-198 improved mitochondria integrity (TMRM staining, Supplementary Fig. S1e), inhibited lipid peroxidation (revealed by BODIPY 581/591 staining, Supplementary Fig. S1f), and reduced abnormal lipid accumulation (revealed by BODIPY 493/503 staining, Supplementary information and Supplementary Fig. S1g) caused by TAA and APAP[39,40]. SCM-198 also increased hepatic glycogen storage, which is depleted in ALF (Supplementary Fig. S1h). Moreover, SCM-198 reduced F4/80$^+$ macrophage infiltration (Fig. 1g and Supplementary Fig. S1i) and decreased serum IL-1β and TNF-α levels (Fig. 1h), suggesting that SCM-198 also attenuates local and systemic inflammation in ALF mice.

The SCM-198-treated livers had significantly more Ki67$^+$ proliferating cells (Fig. 1i and Supplementary Fig. S1j) but fewer TUNEL$^+$ apoptotic cells (Fig. 1j and Supplementary Fig. S1k) than the saline group (at 48 hpi). Immunoblotting analysis confirmed increased levels of CCND1, PCNA, and Bcl2 and decreased levels of cleaved Caspase 3 and Bax in SCM-198 treated livers (Supplementary Fig. S1l), indicating that SCM-198 initiates a regenerative response post-ALF.

These results demonstrated that SCM-198, even when administered at 24 hpi, quickly reverses murine ALF progression.

### Identification of AdipoR2 as a binding partner of SCM-198

To investigate the mechanism of SCM-198 in ALF, we used affinity purification to analyze the SCM-198 binding partners in protein extracts of AML12 mouse hepatocytes. It has been documented that

https://doi.org/10.1038/s41467-024-55295-7

isolated rodent hepatocytes tolerate high concentrations of TAA- or APAP-induced injuries[40,41]. Direct application of TAA or APAP to the AML12 cells did not produce reliable phenotypes. Therefore, we treated the AML12 cells with peroxide ($H_2O_2$) to mimic the oxidative stress in ALF[21,42,43]. First, we demonstrated that the $H_2O_2$-challenged AML12 cells respond to SCM-198. AML12 cells treated with 0.88 μM of $H_2O_2$ exhibited increased lipid peroxidation and abnormal lipid accumulation, which were attenuated by SCM-198 (Supplementary Fig. S2a, b).

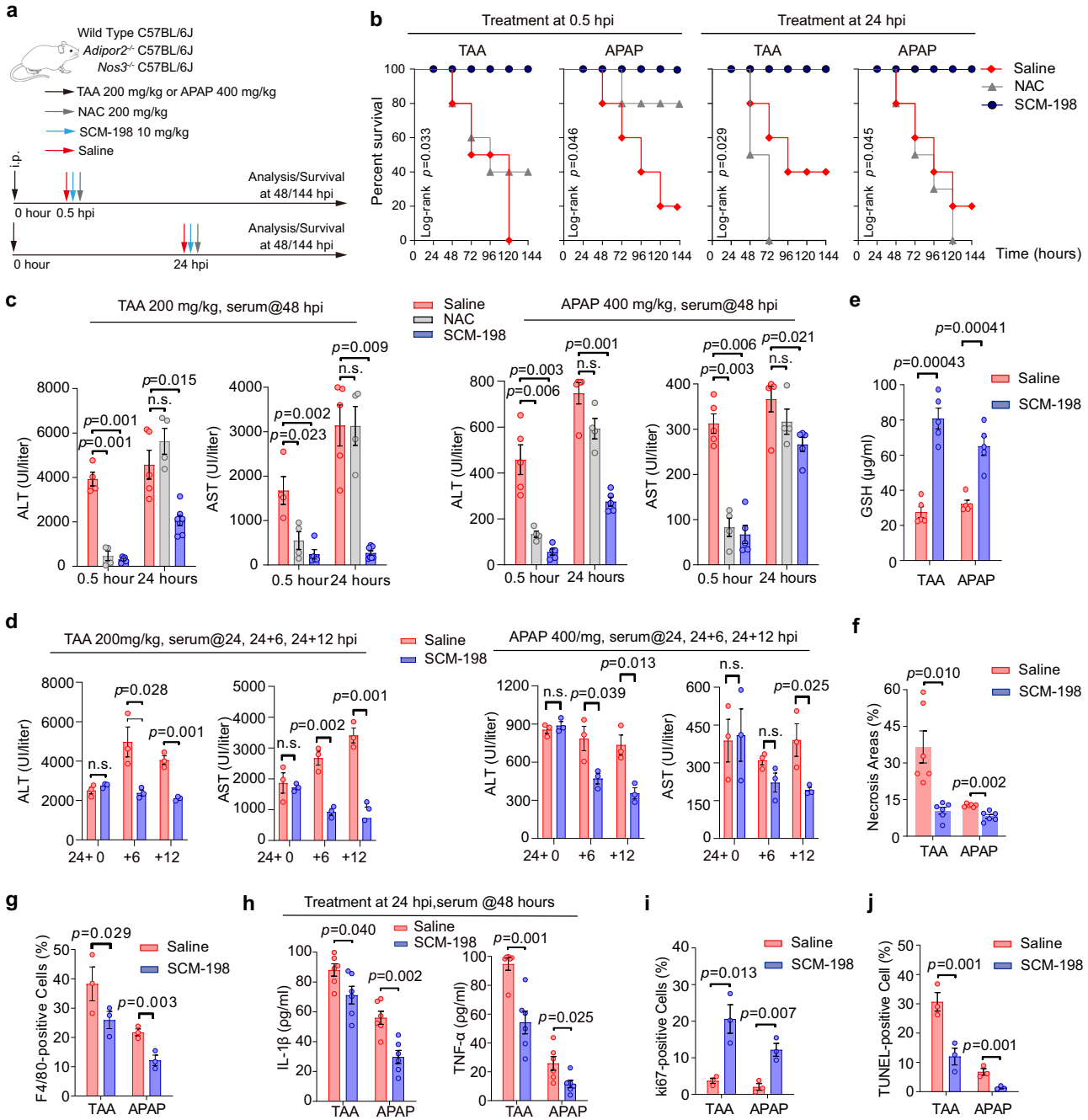


**Fig. 1 | SCM-198 enables the survival of ALF mice. a** Schematics of the TAA- or APAP-induced ALF mouse model used in this study. SCM-198 (10 mg/Kg body weight) or NAC (200 mg/Kg body weight) was given intraperitoneally at 0.5 hpi (hour post-TAA or APAP intoxication/injection, prophylactic) or 24 hpi (therapeutic). Survival of the mice was examined at 144 hpi, and serum/tissue samples were collected at 48 hpi for all experiments, unless stated otherwise. **b** Percent survival chart of WT mice after saline, NAC, or SCM-198 treatment given at 0.5 or 24 hpi ($n = 10$ per group). The *p*-values were determined using the Log-rank test. **c** Serum ALT and AST levels were measured at 48 hpi in WT mice treated with saline, NAC, or SCM-198 0.5 hpi or 24 hpi (for all bar graphs from left to right, $n = 4,4,5, 5,4,7; 4,4,5; 5,4,7; 5,4,5; 4,4,5; 5,4,5; 4,4,5$). **d** Serum ALT and AST levels in TAA or APAP intoxicated WT mice at the time of SCM-198 administration (24 + 0), or 6 and 12 h after SCM-198 administration (24 + 6, 24 + 12). ($n = 4$). **e** GSH concentrations in WT mice liver tissue at 48 hpi ($n = 5$). **f** Quantification analysis of necrosis areas on liver sections at 48 hpi ($n = 6$ mice). **g** Quantification of F4/80+ cells on liver sections at 48 hpi ($n = 3$ mice). **h** Plasma levels of IL-1β and TNF-α detected by ELISA at 48 hpi ($n = 6$ mice). **i** Quantification of Ki67 + cells on liver sections at 48 hpi ($n = 3$ mice). **j** Percentages of TUNEL + cells on liver sections at 48 dpi ($n = 3$ mice). Data in (**c**–**j**) are presented as mean ± SEM. The *p*-values were determined using *t test*, two tails, except in (**b**), which was determined using the Log-rank test. n.s., not significant. Source data are provided as a Source Data file.

https://doi.org/10.1038/s41467-024-55295-7

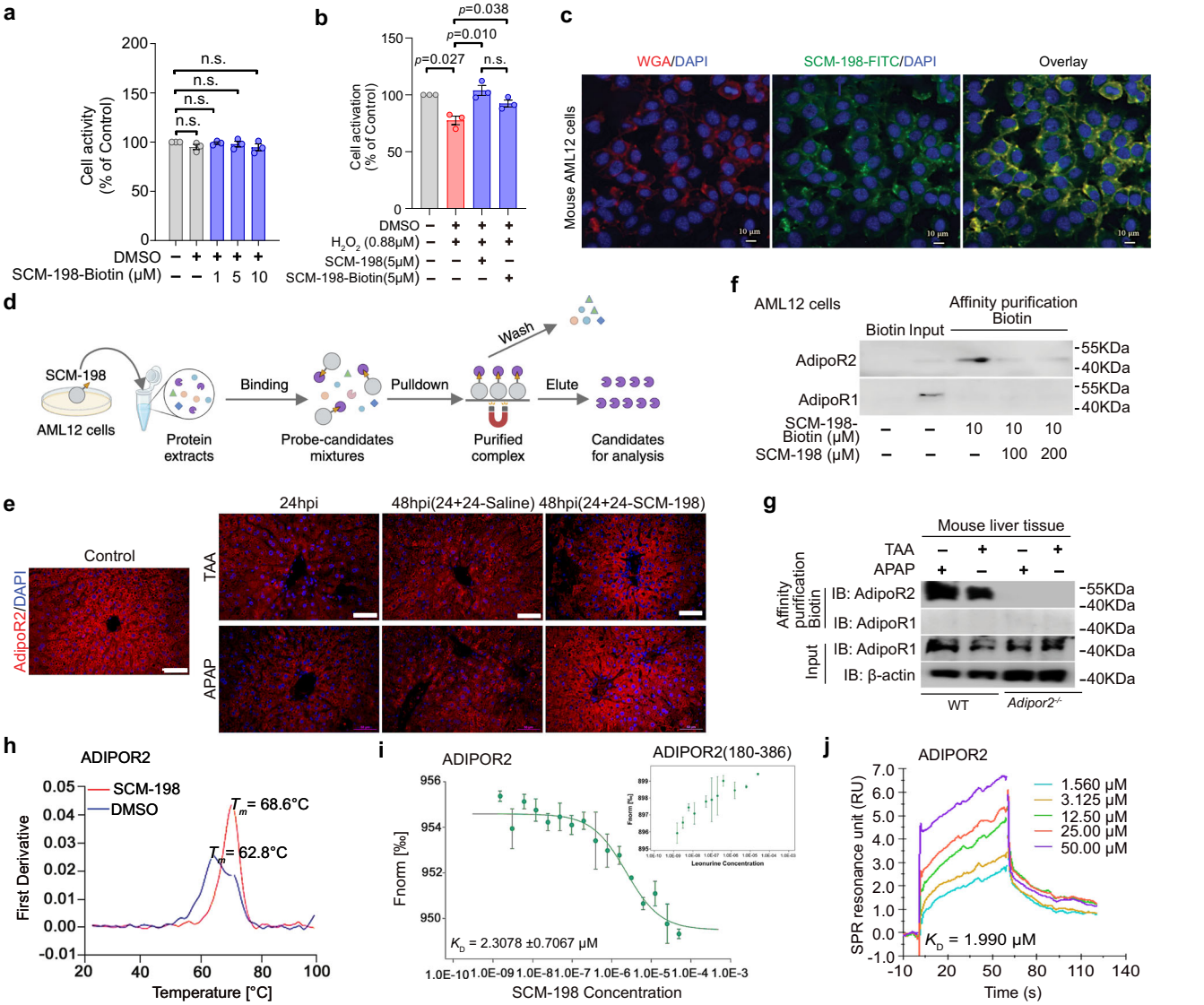


**Fig. 2 | AdipoR2 is a direct binding target of SCM-198. a** Cell activity analysis of AML12 cells treated with different amounts of SCM-198-Biotin, with CCK8 assay. **b** Cell activity analysis of AML12 cells treated with SCM198 or SCM-198-Biotin, after $H_2O_2$ exposure, showing that SCM-198-Biotin had a similar effect to SCM-198. **c** Fluorescence image of mouse AML12 hepatocytes after incubation with SCM-198-FITC (green) at 37 °C for 24 h. The nucleus was stained with DAPI, and the cell membrane was stained with WGA (red). Scale bars, 10 μm. **d** Schematic illustration of the affinity-purification approach for identifying SCM-198 targeting proteins from cytomembrane extracts of AML12 mouse hepatocytes incubated with SCM-198-Biotin probe. Created in BioRender. Lin, G. (2024) https://BioRender.com/s19x956. **e** Immunofluorescence staining of AdipoR2 on liver sections of TAA/APAP-intoxicated mice, 24 and 48 hpi. Mice were given saline or SCM-198 at 24 hpi. Control: uninjured. Scale bar: 50 μm. **f** Immunoblotting of AdipoR2 and AdipoR1 in eluate obtained from AML12 hepatocytes, following the procedure shown in (**d**). Biotin, negative control; Non-labeled SCM-198, a competitor for SCM-198-Biotin. Similar results were obtained from 3 independent repeats. **g** Immunoblotting of AdipoR2 in TAA/APAP- intoxicated WT and *Adipor2*$^{-/-}$ mouse liver tissue extracts, affinity purified with SCM-198-Biotin probes. β-actin was used as the input loading control. **h** Differential scan fluorimetry analysis showing the changes in the enthalpy of recombinant human ADIPOR2 incubated with SCM-198 in PBS buffer at indicated temperatures. *Tm*: thermal transition midpoint. **i** Microscale thermophoresis analysis of the binding affinity between the ADIPOR2 and SCM-198. The fitted $K_d$ value for ADIPOR2-SCM-198 interaction is shown. Error bars indicate the SEM of three separate experiments. ADIPOR2(180-386) was used as control. **j** SPR binding curves and equilibrium fits for the interaction of ADIPOR2 with SCM-198 (at different concentrations). Data in (**a**, **b**) are presented as mean ± SEM. $n = 3$ experimental repeats. *p*-value was determined using SPSS v20 for *t test*, two-tail analysis. n.s., not significant. Similar results were obtained in 3 independent repeats (**c**, **e**, **g**). Source data are provided as a Source Data file.

SCM-198 also increased the percentage of EdU$^+$ cells after $H_2O_2$ exposure (Supplementary Fig. S2a, b). We then obtained SCM-198-FITC for visualizing the localization of SCM-198 in the cells and SCM-198-Biotin for affinity purification of SCM-198-bound proteins. These probes were of high purity (96.69%) and were not toxic to the cells (Fig. 2a). SCM-198-Biotin also showed similar protective effects on AML12 cells from $H_2O_2$ injury (Fig. 2b), indicating that Biotin labeling does not interfere with SCM-198's hepatoprotective function. Using the SCM-198-FITC probe, we observed that SCM-198 binds the cell surface (Fig. 2c). Therefore, we isolated the cytomembrane proteins of AML12 hepatocytes incubated with SCM-198-Biotin probes and performed affinity purification followed by ultra-high-resolution liquid chromatography-mass spectrometry (LC-MS) (Fig. 2d).

From the 386 candidates revealed by the LC-MS analysis (Supplementary Data 1), we screened for membrane-associated proteins (as the SCM-198-FITC probe was localized to the cell surface, Fig. 2c) and identified AdipoR2, Moesin, and Plectin as the highest-scored membrane proteins (Supplementary Table S1). AdipoR2 is one of the two

https://doi.org/10.1038/s41467-024-55295-7

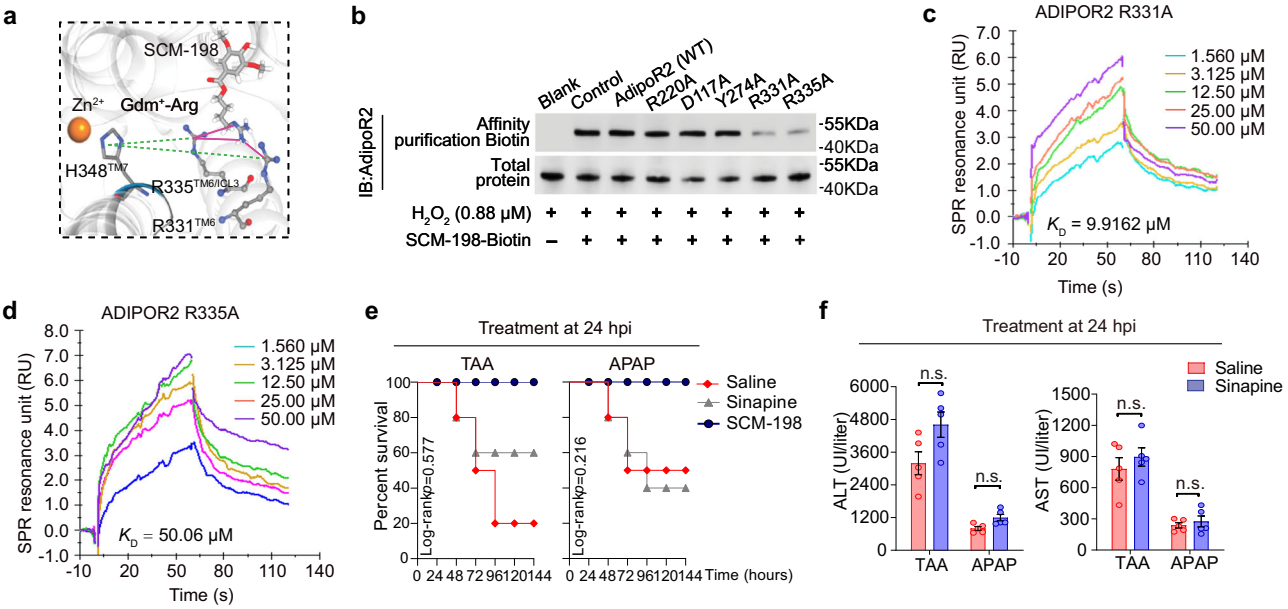


**Fig. 3 | Characterization of SCM-AdipoR2 binding. a** A molecular docking model of SCM-198 binding to AdipoR2, showing the formation of salt bridges (green dotted lines) between R335-H348 (2.3 Å), and potential formation of guanidinium pairing (Gdm$^+$-Arg) between the guanidino groups of SCM-198 and AdipoR2 (R335), shown in magenta lines. **b** Immunoblotting of AdipoR2 in eluates obtained from AML12 hepatocytes overexpressed with *AdipoR2* (WT), or *AdipoR2* mutants, treated with $H_2O_2$, following the procedure shown in (2 **d**). Similar results were obtained in 2 independent repeats. **c**, **d** SPR binding curves and equilibrium fits for the interaction of ADIPOR2 R331A (**c**), or ADIPOR2 R335A (**d**) protein with SCM-198. **e** Percentage of survival of WT mice injected intraperitoneally with saline, SCM-198, or Sinapine (an analog to SCM-198) at 24 hpi ($n = 10$). The *p*-values were determined using the Log-rank test. **f** Serum levels of ALT and AST in TAA/APAP- intoxicated mice at 48 hpi. Mice were treated with saline or Sinapine at 24 hpi. Data in (**f**) are presented as mean ± SEM. $n = 5$ mice. *p*-value was determined using SPSS v20 for *t test*, two-tail analysis. n.s., not significant. Source data are provided as a Source Data file.

adiponectin receptors abundantly expressed in the liver and regulates lipid metabolism[44]. The highest score of AdipoR2 (based on -10lgP), along with SCM-198's effect on lipid accumulation (Fig. 1 and Supplementary Fig. S1), suggests that AdipoR2 is a potential SCM-198 target. Both Moesin and Plectin regulate actin organization and polarity[45,46], and thus may help maintain the epithelial integrity of the hepatocytes rather than mediate SCM-198's effect on lipid accumulation and peroxidation. Therefore, we focused on AdipoR2 for further investigation.

AdipoR2 was expressed on the hepatocyte surface in mouse liver, but its expression was reduced by TAA or APAP injury (both 24 and 48 hpi). However, in the SCM-198-treated mice, AdipoR2 was abundantly expressed in the hepatocytes, with an expression pattern similar to that in normal mice (Fig. 2e). In human liver specimens, ADIPOR2 was also expressed in the hepatocytes, but its expression was disrupted by APAP overdose (Supplementary Fig. S3a).

To confirm that AdipoR2 binds SCM-198 in AML12 cells, we performed the affinity purification in the presence of unlabeled SCM-198 as a "cold" competitor, which reduced the amount of AdipoR2 pulled down by the SCM-198-Biotin probe (Fig. 2f). SCM-198 bound AdipoR2 in the liver tissues after TAA/APAP intoxication, as revealed by the affinity purification from liver tissue extracts (Fig. 2g, wild type (WT) group).

Interestingly, AdipoR1, the other adiponectin receptor expressed in the liver[44], was not identified by LC-MS (Supplementary Data 1). Immunoblotting confirmed that SCM-198-Biotin did not pull down AdipoR1 in the AML12 cells (Fig. 2f), nor WT or *Adipor2*$^{-/-}$ liver tissues after TAA or APAP intoxication (Fig. 2g). These ruled out AdipoR1's involvement in mediating SCM-198's effects in the livers. The pulling down of AdipoR2 by SCM-198-Biotin was not due to Biotin either, as a Metformin-Biotin probe did not pull down AdipoR2 (Supplementary Fig. S3b).

We then expressed and purified full-length human ADIPOR2 recombinant proteins (mouse and human ADIPOR2 proteins are highly conserved) and characterized the binding affinity of ADIPOR2 to SCM-198, using differential scanning fluorimetry (DSF), microscale thermophoresis (MST), and surface plasmon resonance (SPR). ADIPOR2 bound SCM-198 directly in vitro, as revealed by a direct pull-down assay (Supplementary Fig. S3c). DSF showed a shift in the thermal transition midpoint of ADIPOR2 in the presence of SCM-198, from 62.8 °C to 68.6 °C (Fig. 2h). MST and SPR estimated a dissociation constant ($K_d$) of 2.308 μM and 1.99 μM, respectively (Fig. 2i, j). These values are within the range of intracellular concentrations of SCM-198 detected in mice or rhesus monkeys administered with regular doses[34,47,48].

## SCM-198 binds AdipoR2 through guanidinium pairing with residue R335

To gain more insight into the molecular basis of SCM-198 interaction with AdipoR2, we performed molecular dynamics simulations and ultrahigh-resolution LC-MS to identify the key binding residues in AdipoR2. In-silico modeling with human ADIPOR2 (PDB: 6KS1) suggested that SCM-198 could interact with ADIPOR2 through the residues arginine 278 (R278$^{TM5}$), R331$^{TM6}$, R335$^{TM6/ICL3}$; R331$^{TM6}$ and R335$^{TM6/ICL3}$ may activate H348$^{TM7}$ by forming a salt bridge (Fig. 3a and Supplementary Fig. S4a, b). LC-MS analysis with the affinity purification eluate from AML12 cells treated with SCM-198-Biotin (Supplementary Fig. S4c) and ADIPOR2 proteins affinity-pulled down by SCM-198-Biotin from an in vitro binding assay (Supplementary Fig. S4d) showed that R335 was the major residue of AdipoR2 modified by SCM-198 (with an increase of m/z of 311.33).

In addition to R335, another residue bound by SCM-198 was R331 (Supplementary Fig. S4d). To investigate the importance of these residues, we generated point mutations of AdipoR2 R331A and R335A (arginine to alanine) and examined SCM-198 binding in AML12 cells overexpressing wild type (WT) or mutated AdipoR2 DNA. Both R331A and R335A mutations impaired SCM-198 binding with AdipoR2 (Fig. 3b). SPR analysis with purified ADIPOR2 R331A and ADIPOR2 R335A proteins revealed that the mutation of R331A and R335A of

https://doi.org/10.1038/s41467-024-55295-7

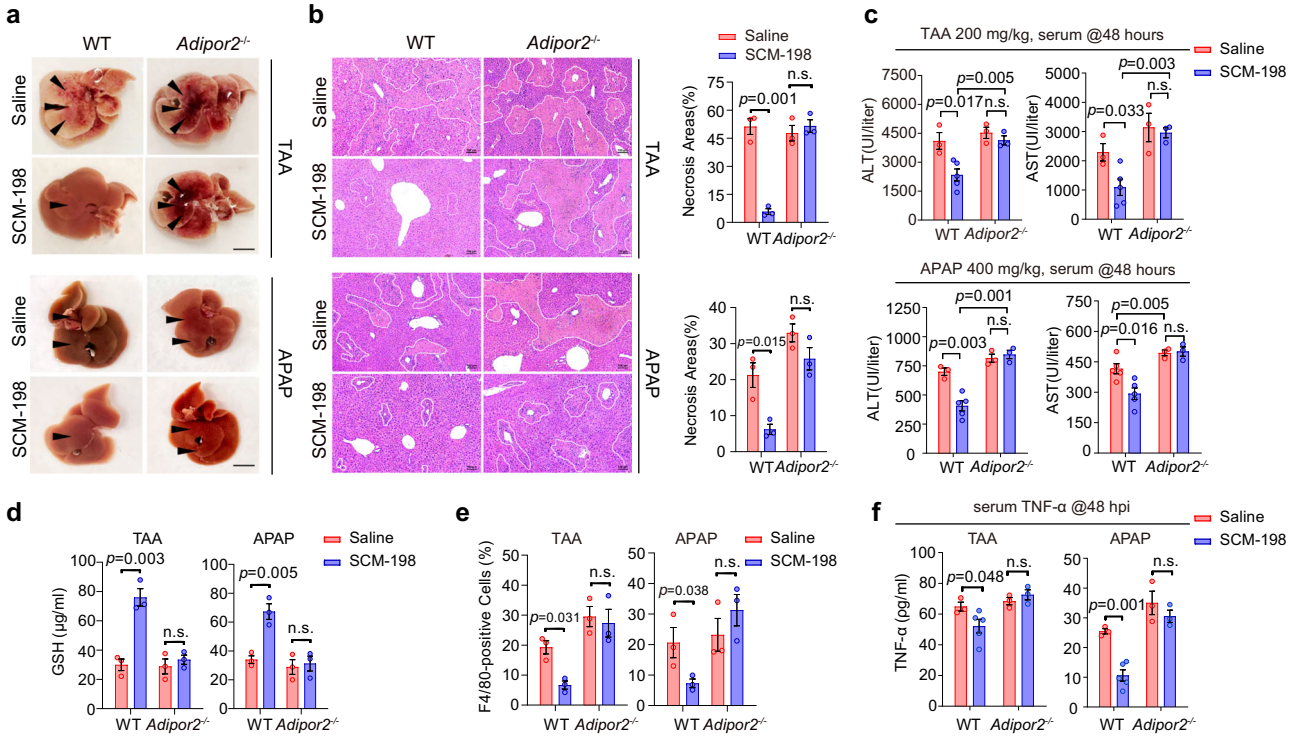


**Fig. 4 | AdipoR2 deficiency abolishes the protective effect of SCM-198 on ALF models. a** Representative photograph of WT and *Adipor2*$^{-/-}$ mouse livers (48 hpi). SCM-198 was given at 24 hpi (in **a**–**f**). Black arrowheads indicate sites of severe lesions. Scale bars, 5 mm. **b** HE staining and quantification analysis on WT and *Adipor2*$^{-/-}$ mouse liver sections, 48 hpi. Scale bars, 100 μm. **c** Serum levels of ALT and AST, measured at 48 hpi in WT and *Adipor2*$^{-/-}$ TAA/APAP-intoxicated mice. **d** Quantification of GSH in liver tissues of WT and *Adipor2*$^{-/-}$ mice, 48 hpi. **e** Quantification of F4/80 + cells on WT and *Adipor2*$^{-/-}$ mouse liver sections, 48 hpi. **f** Serum TNF-α measured at 48 hpi in WT or *AdipoR2*$^{-/-}$ mice treated with saline or SCM-198 at 24 hpi. Data in (**b**–**f**) are presented as mean ± SEM. $n = 3$ mice in (**b**, **d**, **e**). $n = 3$-5 mice in (**c**, **f**, $n = 5$ in WT/SCM-198 group, $n = 3$ in all other groups). The *p*-values were determined using SPSS v20 for *t test*, two-tail analysis. n.s., not significant. Source data are provided as a Source Data file.

ADIPOR2 increased the *Kd* values to 9.92 μM and 50.06 μM ( ~ 25-fold increase compared to AdipoR2 WT), respectively (Fig. 3c, d). These results indicated that the R335 residue is important for SCM-198-AdipoR2 binding.

We performed two experiments to confirm the role of R335 in mediating the function of SCM-198. First, we generated *AdipoR2* knockout (*Adipor2*$^{-/-}$) AML12 cells and reintroduced AdipoR2 R335A or AdipoR2 WT (Supplementary Fig. S5a), and examined the effect of SCM-198 on attenuating $H_2O_2$-induced stress injury. SCM-198 attenuated the abnormal lipid accumulation when AdipoR2 WT was reintroduced, but not in the case of AdipoR2 R335A (Supplementary Fig. S5b, c). Nor could it promote cell proliferation in AdipoR2 R335A-overexpressing *Adipor2*$^{-/-}$ cells (Supplementary Fig. S5b, d). Second, our structural activity relationship analysis predicted that guanidinium pairing ($Gdm^+$-Arg) might occur between SCM-198 and AdipoR2 R335 within a 4 Å distance, which could increase the dielectric constant (ε) by over 8-fold (Fig. 3a and Supplementary Fig. S4b), with a stabilizing effect of higher ε[49] that may increase the affinity of AdipoR2-SCM-198 binding. To test whether this hypothesized guanidinium pairing is important for the AdipoR2-SCM-198 binding and the activation of AdipoR2 signaling, we utilized Sinapine as an analog to SCM-198 to compare its hepatoprotective effect in TAA/APAP-induced ALF mice. Sinapine has quaternary amine instead of amide in SCM-198 and thus cannot form guanidinium pairing with Arginine (Supplementary Fig. S6a). In the AML12 hepatocytes exposed to $H_2O_2$, Sinapine failed to protect the AML12 cells from death (Supplementary Fig. S6b) or prevent the deaths of the TAA/APAP-induced ALF mice (Fig. 3e). The serum ALT or AST levels were not reversed by Sinapine either (Fig. 3f). These results suggested that the guanidine-arginine pairing between AdipoR2 R335 and SCM-198 is critical for SCM-198-AdipoR2 binding and signaling.

## AdipoR2 is required for the protective effect of SCM-198 in murine ALF

The above results demonstrated that *Adipor2*$^{-/-}$ AML12 cells no longer respond to SCM-198 treatment. This was also evident in AML12 cells after the knocking down of AdipoR2 with *Adipor2* siRNA (Supplementary Fig. S7a–c). SCM-198 upregulated AdipoR2 expression in the AML12 hepatocytes after $H_2O_2$ exposure and increased the level of ACC1(pS79), the key enzyme in the biosynthesis and oxidation of fatty acids. However, this effect of SCM-198 was abolished by *Adipor2* siRNA (Supplementary Fig. S7d). SCM-198 dose-dependently decreased the expression of cCaspase-3 and Bax, and increased Bcl2 expression (Supplementary Fig. S7e), which were all diminished by *Adipor2* siRNA (Supplementary Fig. S7f).

Then, we used *Adipor2*$^{-/-}$ mice (Supplementary Fig. S8a–c) to examine the effect of SCM-198 on treating ALF upon the complete loss of AdipoR2. In contrast to the WT mice, high levels of necrosis persisted in the SCM-198-treated and saline-treated *Adipor2*$^{-/-}$ livers (Fig. 4a, b). SCM-198 treatment in the *Adipor2*$^{-/-}$ mice could no longer decrease serum ALT and AST levels (Fig. 4c) or increase the level of GSH in liver tissues (Fig. 4d). The SCM-198-treated *Adipor2*$^{-/-}$ livers also displayed severe sterile inflammation, with more macrophage activation (Fig. 4e and Supplementary Fig. S8d), and high serum TNF-α levels (Fig. 4f). The effect of SCM-198 on inhibiting cell death or increasing cell proliferation was also abolished in *Adipor2*$^{-/-}$ mice, as analyzed by TUNEL staining, $Ki67^+$ counting, or western blotting assay of cCaspase-3, Bax, Bcl2, PCNA, and P21 (Supplementary Fig. S8e–i). These in vitro and in vivo experiments

demonstrated that AdipoR2 mediates the hepatoprotective effect of SCM-198 in the liver.

### SCM-198-AdipoR2 interaction increases NO production through NOS3

To understand the downstream molecular mechanism of AdipoR2 after SCM-198 treatment in ALF, we performed RNA-sequencing of the liver tissues after SCM-198 treatment in WT APAP-injured mice. Gene ontology (GO) analysis of the 710 differentially expressed genes (DEGs) revealed that SCM-198 could act through the regulation of the endothelial cell apoptosis process, inflammatory response, and lipid metabolism (Supplementary Fig. S9a). The upregulated genes were involved in the negative regulation of cell death, consistent with the earlier results (Fig. 1 and Supplementary Fig. S1). Notably, SCM-198-upregulated genes were involved in nitric oxide (NO) production and the response to calcium (Supplementary Fig. S9a).

NO is an important signaling molecule in tissue repair and regeneration[50–52]. NO deficiency impairs liver regeneration after resection[53], and a moderate NO level is essential for liver regeneration after partial hepatectomy[54]. Therefore, we explored the effect of SCM-198 on NO production. In AML12 hepatocytes, SCM-198 increased the intensity of DAF-FM DA, an indicator for NO content (Fig. 5a). SCM-198 maintained the NO levels in AML12 cells, which was decreased by $H_2O_2$, but this effect was abolished by AdipoR2 siRNA (Fig. 5b and Supplementary Fig. S9b). In the mouse livers, NO content was significantly reduced by TAA at 24 hpi but was restored by SCM-198 at 48 hpi. NO content was transiently increased by APAP at 24 hpi but was lowered at 48 hpi in the saline-treated group and increased in the SCM-198 group (Fig. 5c). SCM-198 failed to increase the NO content in *Adipor2*$^{-/-}$ mice after TAA /APAP intoxication (Fig. 5d and Supplementary Fig. S9c, d). Thus, SCM-198 regulates NO levels through the AdipoR2 signaling pathway.

To confirm the role of NO in mediating the effect of SCM-198-AdipoR2 signaling in ALF, we inhibited the activity of nitric oxide synthases (NOS) with L-NAME in AML12 cells and ALF mice. L-NAME nullified the increase of NO production elicited by SCM-198 (Fig. 5e). And in mice injected with L-NAME, SCM-198 failed to protect the liver from necrosis after TAA/APAP intoxication, as evidenced by the histology analysis and serum ALT and AST levels (Supplementary Fig. S9e–h and Fig. 5f, g).

To identify which NOS mediates NO production in SCM-198-treated hepatocytes, we overexpressed AdipoR2 in BNL CL.2 hepatocytes (low AdipoR2-expressing). We found that the phosphorylated NOS3(pS1177), the most critical phosphorylated form of NOS3 for NO synthesis[55], was increased by AdipoR2 (Fig. 5h). Yet, the level of NOS2 was not significantly changed by AdipoR2 overexpression. Our LC-MS analysis also detected NOS3 in the affinity purification eluate pulled down by SCM-198 (Supplementary Data 1). In mouse livers, TAA/APAP injury decreased the phosphorylation levels of NOS3(pS1177) and CaMKII (pT286), but these levels were restored by SCM-198 (Fig. 5i). It is established that CaMKII can phosphorylate NOS3, and phosphorylation of NOS3 at Ser1177 enhances its enzymatic activity to produce NO[56]. Thus, these results indicated that NOS3 is involved in SCM-198-elevated NO production.

We utilized the *Nos3*$^{-/-}$ TAA ALF model to confirm the role of NOS3 in mediating the protective effect of SCM-198. Uninjured *Nos3*$^{-/-}$ livers had much lower intensity of NO, which could not be increased by SCM-198 (Fig. 5j). After TAA/APAP intoxication, the *Nos3*$^{-/-}$ mice were no longer protected by SCM-198 treatment, resulting in severe necrosis (Fig. 5k, l), high levels of serum ALT and AST (Fig. 5m), and low level of liver tissue GSH (Fig. 5n).

As an important messenger molecule, NO has anti-inflammatory and anti-oxidant effects[50,54,57]. As expected, *Nos3*$^{-/-}$ liver tissues had a high percentage of F4/80 positive cells (Fig. 5o) and high levels of IL1-β and TNFα, which were not attenuated by SCM-198 (Fig. 5p). Consequently, there were high levels of apoptosis and low level of proliferation in the *Nos3*$^{-/-}$ injured liver tissues (Fig. 5q, r and Supplementary Fig. S9i). In addition, NO has also been suggested to regulate fatty acid oxidation (FAO). In zebrafish and rats, the application of NO donors has been shown to impact FAO in the liver[58,59]. To examine whether SCM-198 also affects fatty acid oxidation (FAO), we performed lipidomics analysis in AML12 cells after $H_2O_2$ exposure. This revealed that there was an aberrant accumulation of FA16:0 and FA18:0 caused by $H_2O_2$ injury, but SCM-198 could reverse the increase of these fatty acids (Supplementary Fig. S10), consistent with the effect of SCM-198 on lipid accumulation (Supplementary Fig. S1) and the role of NO in terminating lipid peroxidation[57]. Thus, the hepatoprotective function of SCM-198 in treating ALF is mediated by the NOS3-NO axis.

### An AdipoR2-CaM-CaMKII-NOS3 complex directly mediates the effect of SCM-198

We sought to understand how SCM-198 transduces AdipoR2 signaling to produce NO in the injured liver. While adiponectin can activate NOS3 in vascular endothelial cells through the mTOR or AMPK pathways[36,60,61], our analysis showed that the levels of mTOR (pS2448) and pAMPK were not significantly affected by SCM-198 in AML12 cells (Supplementary Fig. S11a). SCM-198 did not increase cAMP levels (Supplementary Fig. S11b), or alter the expression levels of the cAMP protein kinase catalytic subunit (PRKACA) in AML12 hepatocytes challenged with $H_2O_2$ or in liver tissues after TAA/APAP intoxication (Supplementary Fig. S11c, d). These results suggested that the mTOR and AMPK pathways are not the primary pathways responsible for the SCM-198-induced NO production.

LC-MS analysis revealed that in addition to NOS3, CaM was also pulled down by the SCM-198-Biotin probe (Supplementary Table S1). It has been shown that NOS3 activity can be regulated by $Ca^{2+}$/Calmodulin (CaM)/CaMKII, and CaM can bind to NOS3[56,62,63]. This raised the possibility that SCM-198 regulates NOS3 directly by forming a complex. Indeed, immunoprecipitation of AdipoR2 pulled down CaM, CaMKII, and NOS3 in normal or injured mouse liver tissues (Fig. 6a) and in AML12 hepatocytes (Fig. 6b). Immunoprecipitation of CaM pulled down AdipoR2, NOS3, and CaMKII (Fig. 6c). Thus, we identified a new complex in which AdipoR2 interacts with a known NO-producing CaM-CaMKII-NOS3 complex by directly binding to CaM and NOS3, both in normal and injured liver. We further identified the interaction domains of AdipoR2 and NOS3 by coimmunoprecipitation experiments with overexpression of a series of deletion constructs of *NOS3* and *Adipor2* in AML12 cells (Supplementary Fig. S12a). This showed that the intracellular fragment of AdipoR2 ($AdipoR2^{1\text{-}146}$) binds the C-terminal part of NOS3 ($NOS3^{753\text{-}1203}$) (Fig. 6d, e and Supplementary Fig. S12b).

To confirm that SCM-198's effect on NO production is mediated by CaM and CaMKII, we used the CaM antagonist R24571 and the CaMKII inhibitor KN93. Both abolished the increase of NOS3(pS1177) by SCM-198 under $H_2O_2$ exposure (Fig. 6f,g) and abolished the effect of SCM-198 on NO production (Fig. 6h). Similarly, BAPTA-AM ($Ca^{2+}$ chelator) significantly reduced the levels of NOS3(pS1177) (Fig. 5g), and abolished SCM-198's effect on regulating NO production (Fig. 6h). Moreover, R24571, KN93, and BAPTA-AM abolished the effect of SCM-198 on attenuating ROS production, which was significantly increased by $H_2O_2$ exposure (Supplementary Fig. S13a, b). These findings indicated that the activity of SCM-198 relies on $Ca^{2+}$/CaM-CaMKII activation.

Interestingly, phosphorylation of NOS3 (pS1177) and CaMKII(pT286) was not affected by Cycloheximide (CHX), which binds the 60S ribosomal subunit to inhibit protein synthesis[64] (Figs. 6i, 6 h after CHX treatment). SCM-198-induced NO production was also not affected by CHX (Fig. 6j), suggesting that SCM-198-AdipoR2 signaling transduction does not require new protein synthesis.

https://doi.org/10.1038/s41467-024-55295-7

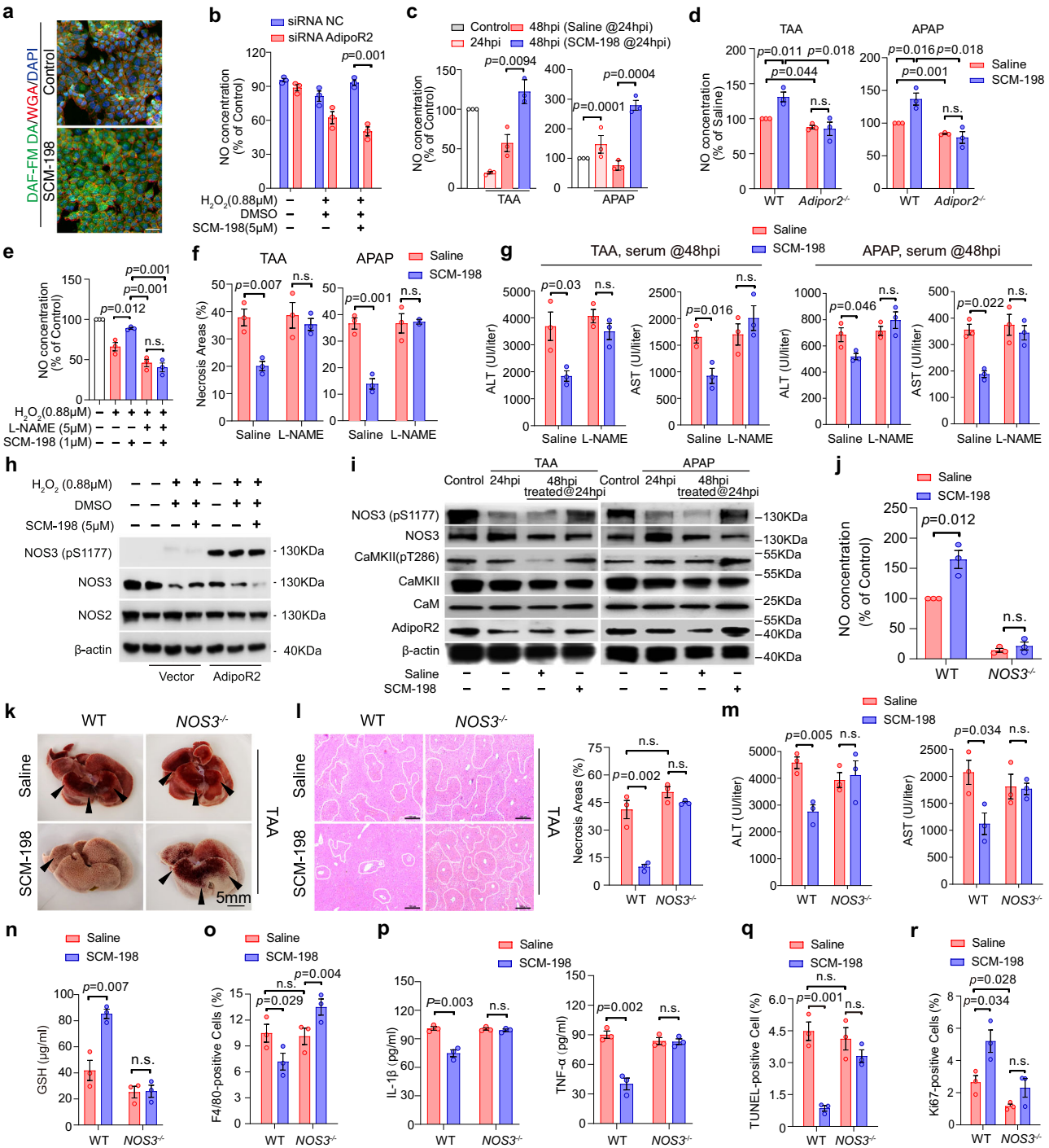


**Fig. 5 | SCM-198 regulates NO production through NOS3. a** Detection of NO with DAF-FM DA (green) in control or SCM-198 treated AML12 cells. Scale bar, 20 μm. **b** NO content of the AML12 cells transfected with *Adipor2* siRNA or negative control siRNA. Cells were treated with DMSO or SCM-198 for 24 h after $H_2O_2$ exposure. **c** NO content of the TAA/APAP-induced ALF mouse liver tissues measured at 48 hpi. Injured mice were treated with saline or SCM-198 at 24 hpi (in **c**, **d**, **f**, **g**, **i**–**r**). **d** NO content of WT and *Adipor2*$^{-/-}$ liver tissues, after TAA/APAP-induced ALF, measured at 48 hpi, normalized to the saline-treated group. **e** NO content of AML12 cells, with or without L-NAME. **f** Quantification of necrosis on liver sections of WT and *Nos3*$^{-/-}$ mice, 48hpi. **g** Serum ALT, AST levels in WT and *Nos3*$^{-/-}$ mice, 48 hpi. **h** Immunoblotting of NOS2, NOS3, and NOS3 (pS1177) in BNL CL.2 cells with or without AdipoR2 overexpression. β-actin as loading control. **i** Immunoblotting of AdipoR2, NOS3, NOS3(pS1177), CaMKII, CaMKII(pT286), and CaM in TAA/APAP-induced ALF mouse liver tissue at 24 and 48 hpi. **j** NO contents in liver tissues in WT and *Nos3*$^{-/-}$ mice at 48 hpi. **k** Representative photographs of WT and *Nos3*$^{-/-}$ livers (48 hpi after TAA injection). Black arrowheads indicate sites of severe lesions. Scale bars, 5 mm. **l** HE staining of WT and *Nos3*$^{-/-}$ liver sections and quantification of necrosis area, 48 hpi. Scale bars, 100 μm. **m** Serum ALT and AST levels in WT and *Nos3*$^{-/-}$ mice, 48 hpi. **n** GSH contents in WT and *Nos3*$^{-/-}$ liver tissues, 48 hpi (TAA). **o** Percentage of F4/80 positive cells in WT and *Nos3*$^{-/-}$ liver, 48 hpi. **p** IL-1β and TNF-α levels in WT and *Nos3*$^{-/-}$ liver tissues. **q**, **r** Percentage of TUNEL$^{+}$ cells (**q**), Ki67$^{+}$ cells (**r**) on WT and *Nos3*$^{-/-}$ liver sections, 48 hpi. Data in (**b**–**g**, **j**, **l**–**r**) are presented as mean ± SEM ($n = 3$ mice). The *p*-values were determined using SPSS v20 for *t test*, two-tail analysis. n.s., not significant. Similar results were obtained in 2 independent repeats in (**a**, **h**, **i**). Source data are provided (Source Data file).

https://doi.org/10.1038/s41467-024-55295-7

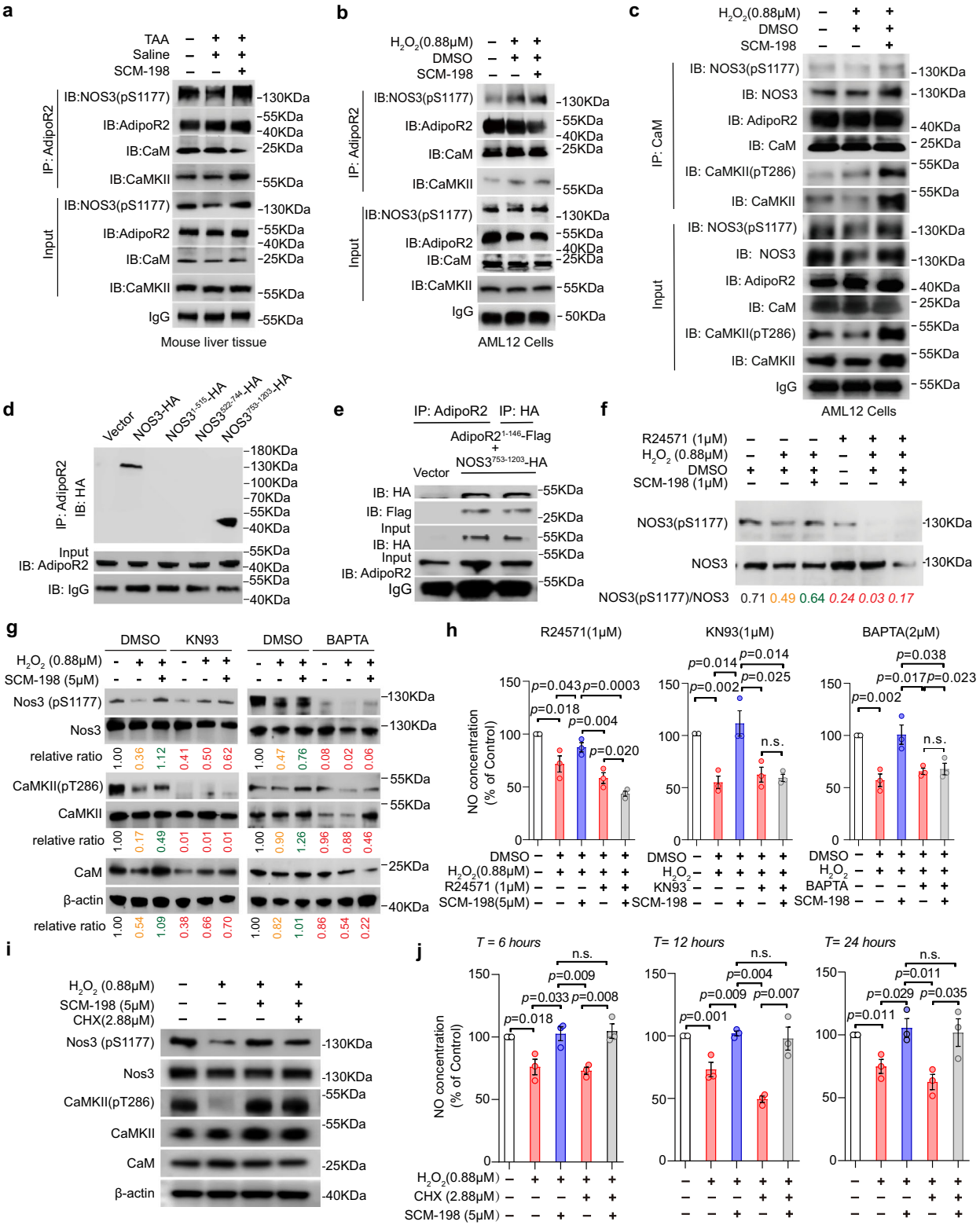


## SCM-198 induces $Ca^{2+}$ influx through AdipoR2 Y274

The above observation suggested that SCM-198 activation of AdipoR2 involves $Ca^{2+}$ influx. Molecular modeling of the human ADIPOR2 (PDB ID: 6KS1) revealed a cavity accessible to $Ca^{2+}$ (Supplementary Fig. S4b). GO analysis of the DEGs also indicated that SCM-198 upregulated the $Ca^{2+}$ response (Supplementary Fig. S9a). To test whether the binding of SCM-198 to AdipoR2 causes $Ca^{2+}$ influx, we investigated the intracellular $Ca^{2+}$ dynamics in $H_2O_2$-exposed AML12 hepatocytes with Fluo-4 AM staining and $Ca^{2+}$ content detection. SCM-198 reversed the $H_2O_2$-induced $Ca^{2+}$ decrease (Fig. 7a) in a dose-dependent manner (Fig. 7b). The SCM-198-induced $Ca^{2+}$ influx was dependent on extracellular $Ca^{2+}$ as BAPTA-AM ($Ca^{2+}$ chelator) abolished the influx response (Fig. 7c; Supplementary Fig. S14a). To determine if SCM-198-induced $Ca^{2+}$ influx depends on AdipoR2, we used siRNA to knock down *Adipor2*, which abolished SCM-198's effect on intracellular $Ca^{2+}$ levels (Fig. 7d and Supplementary Fig. S14b, c). Moreover, SCM-198 increased

**Fig. 6 | Identification of the AdipoR2-CaM-CaMKII-NOS3 complex.** **a**, **b** Immunoblotting of NOS3(pS1177), AdipoR2, CaM, and CaMKII following immunoprecipitation of AdipoR2 in liver tissues of control, or TAA-intoxicated mice at 48 hpi (**a**), or AML12 hepatocytes treated with or without SCM-198 after $H_2O_2$ exposure (**b**). TAA-intoxicated mice (**a**) were treated with saline or SCM-198 at 24 hpi. **c** Immunoprecipitation of CaM followed by immunoblotting of NOS3, NOS3(pS1177), AdipoR2, CaMKII, CaMKII(pT286) and CaM in AML12 hepatocytes treated with or without SCM-198 after $H_2O_2$ exposure. **d** Immunoprecipitation of AdipoR2 in AML12 hepatocytes overexpressing NOS3-HA, NOS3 segments, followed by immunoblotting of HA, showing that AdipoR2 interacts with $NOS3^{FL}$ and the $NOS3^{753\text{-}1203}$ segment. **e** Immunoprecipitation of AdipoR2 or HA in AML12 hepatocytes overexpressing $AdipoR2^{1\text{-}146}$-Flag and $NOS3^{753\text{-}1203}$-HA, followed by immunoblotting with HA and Flag antibody, showing $AdipoR2^{1\text{-}146}$ binds to the $NOS3^{753\text{-}1203}$ segment. **f** Immunoblotting of NOS3(pS1177) and NOS3 in the presence of R24571 and SCM-198, after $H_2O_2$ exposure. Numbers below the bands indicate the ratios of NOS3(pS1177)/NOS3, and significant decreases are shown in red italics. **g** Immunoblotting of NOS3, NOS3(pS1177), CaMKII, CaMKII(pT286) and CaM in AML12 hepatocytes treated with KN93 or BAPTA, after $H_2O_2$ exposure, with or without SCM-198. The relative ratio of NOS3(pS1177)/NOS, CaMKII(pT286)/CaMKII and CaM/β-actin were shown. **h** Relative NO concentration of AML12 cells after $H_2O_2$ exposure and treatment with SCM-198, in the presence of R24571 (a CaM antagonist, 1 μM), or KN93 (an inhibitor of CaMKII, 1 μM), or BAPTA ($Ca^{2+}$ chelator, 2 μM). **i** Immunoblotting of NOS3(pS1177), CaMKII(pT286), NOS3, CaMKII, CaM in AML12 cells exposed to $H_2O_2$ and treatment with SCM-198, in the presence of Cycloheximide (2.88 μM). **j** NO concentration of AML12 cells detected at 6, 12, and 24 h after $H_2O_2$ exposure and treatment with SCM-198, in the presence of Cycloheximide (2.88 μM). Data in (**h**, **j**) are presented as mean ± SEM ($n = 3$ experimental repeats). The *p*-values were determined using SPSS v20 for *t test*, two-tail analysis. ns, not significant. Similar results were obtained in 2 independent repeats (**a**–**g**, **i**). Source data are provided as a Source Data file.

intracellular $Ca^{2+}$ levels in liver tissues of WT, but not *Adipor2*$^{-/-}$, mice (Supplementary Fig. S14d), indicating that SCM-198-induced $Ca^{2+}$ influx was indeed dependent on AdipoR2.

Previous structural biology studies showed that the $R275^{TM5}$-$D117^{N\text{-terminus}}$ interaction in AdipoR2 regulates lipid and ion transport[65–67]. Atomic dynamics simulation showed that the hydroxyl of the Y274 residue could form hydrogen bonds with the carbonyl of SCM-198, increasing the hydrophobicity of the R275 residue and destabilizing $R275^{TM5}$-$D117^{N\text{-terminus}}$ configurations, allowing AdipoR2 to adopt an open conformation (Fig. 7e)[65,66]. Thus, Y274 could serve as a switch for the $Ca^{2+}$ inflow. LC-MS analysis confirmed that the Y274 of AdipoR2 was indeed bound by SCM-198 (Fig. 2d and Supplementary Fig. S4c, d).

To determine whether AdipoR2 Y274 is important for the $Ca^{2+}$ influx induced by SCM-198, we isolated hepatocytes from *Adipor2*$^{-/-}$ mice (Supplementary Fig. S15a) and transfected them with *Adipor2* (WT) or *Adipor2* (Y274A) point mutation DNA constructs (Supplementary Fig. S15b), followed by $H_2O_2$ exposure and SCM-198 treatment. Time-course measurement of Flow-4 AM fluorescence ($Ca^{2+}$ indicator) showed that *Adipor2*$^{-/-}$ primary hepatocytes overexpressed with AdipoR2 (WT) responded to SCM-198, with a continued increase of signals (Fig. 7f). But the Flow-4 AM fluorescence signals were unaltered by SCM-198 in *Adipor2*$^{-/-}$ hepatocytes overexpressed with AdipoR2 (Y274A), and the signals were higher than in the case of AdipoR2 (WT) overexpression (Fig. 7f). This was confirmed by measuring of $Ca^{2+}$ contents of the *Adipor2*$^{-/-}$ hepatocytes (Fig. 7g). Consistently, NO content was also higher in AdipoR2 (Y274A)-expressing cells, which was not altered by SCM-198 (Fig. 7h). These results demonstrated that Y274 is critical for SCM-198-induced $Ca^{2+}$ influx through AdipoR2. Based on these observations, we propose a model in which liver injuries reduce the activity of the AdipoR2/CaM/CaMKII-NOS3 complex. SCM-198, through binding to AdipoR2, promotes Ca2+ influx and increases the CaMKII-NOS3 activity and NO production (Fig. 7i).

## SCM-198 has a hepatoprotective function in an inflammatory ALF model

To explore whether SCM-198 can be used in ALF caused by severe infection and inflammation, we utilized the LPS/D-GalN-induced ALF model[31–33]. We treated the mice with SCM-198 in a similar manner as in the TAA-/APAP- induced ALF mice (Fig. 8a). As the AdipoR2/CaM/CaMKII-NOS3 complex exists in the hepatocytes under either normal or injury conditions, we hypothesized that SCM-198 could also protect the LPS/D-GalN-induced ALF mice. Indeed, all mice survived under SCM-198 treatment administered 24 hpi (Fig. 8b, SCM-198:100%; saline:40%; NAC:20%), with their serum ALT/AST levels reversed (Fig. 8c), as early as 6 h post-treatment (Fig. 8d). Histology analysis (Fig. 8e, f), detection of F4/80, TUNEL and Ki67 immunofluorescence analyses also confirmed the protective effect of SCM-198 on LPS/D-GalN-induced ALF mice (Fig. 8g). As expected, SCM-198 decreased serum levels of IL-1β and TNF-α (Fig. 8h), attenuated abnormal lipid accumulation and peroxidation (Fig. 8i), increased serum level of GSH (Fig. 8j) and NO content in liver tissues (Fig. 8k). SCM-198 also increased the levels of phosphorylated CaMKII(pT286) and NOS3(pS1177). SCM-198 increased expression of PCNA and Bcl2 but inhibited expression of Bax (Fig. 8l). These results indicated that activation of AdipoR2 signaling by SCM-198 can also treat murine inflammatory ALF models.

## SCM-198 protects human liver organoids from oxidative stress and TAA/APAP injury

Since ADIPOR2 expression is disrupted in human APAP injury (Supplementary Fig. S3a), we utilized human liver organoids (HLOs) to explore the potential of SCM-198 for treating human ALF. HLOs have been shown to recapitulate ALF pathology progression and are considered a more reliable model than hepatocyte cultures for drug evaluation[68–73]. We derived HLOs from the H9 human embryonic stem cells following established protocols[71] (Fig. 9a). After 25 days of culture, H9-HLOs expressed HNF4A and CYP2E1 (Fig. 9b). ADIPOR2 was also expressed, mainly on the cell surface (Fig. 9c). To examine SCM-198's protective effect on HLOs upon oxidative stress, we treated the HLOs with $H_2O_2$ for 24 h and performed biochemical analysis. Immunoblotting showed that the level of phosphorylated NOS3 (pS1177) in HLOs was reduced by $H_2O_2$ but restored by SCM-198 (Fig. 9d). SCM-198 also increased the NO content in the HLOs (Fig. 9e). In terms of the function of HLOs, SCM-198 restored the GSH levels (Fig. 9f) and decreased the level of ALT and AST elevated by $H_2O_2$ (Fig. 9g). Furthermore, SCM-198 reduced TNF-α, IL-1β, and TGF-β1 secretion from $H_2O_2$-treated HLOs (Fig. 9h).

Then, we examined the effect of SCM-198 on the HLOs after TAA/APAP intoxication. After a series of titration, we established a protocol that includes a combination of 5 μM of TAA or 50 μM of APAP and 10 μM of SCM-198 for treating HLOs. After 24 h of incubation, we collected the medium and HLO lysis for analysis. TAA / APAP treatment increased the ALT and AST levels in the HLO medium (normalized to HLO protein contents), suggesting the suitability of HLOs in evaluating the effect of SCM-198 (Fig. 9i, j). SCM-198 reduced the levels of ALT and AST back to controls (Fig. 9i, j). As in the liver tissues, SCM-198 increased the phosphorylation levels of NOS3 (pS1177) and CaMKII (pT286) in HLOs (Fig. 9k). SCM-198 also restored $Ca^{2+}$ concentration and NO contents in TAA- or APAP-injured HLOs (Fig. 9l, m). In addition, SCM-198 increased the levels of PCNA, Bcl2, and CCND1 but decreased the level of p21, cCaspase-3, and Bax proteins in HLOs (Fig. 9n). These observations demonstrated that SCM-198 acts similarly in the HLOs as in the mouse livers, raising the therapeutic potential of SCM-198 in treating human ALF.

https://doi.org/10.1038/s41467-024-55295-7

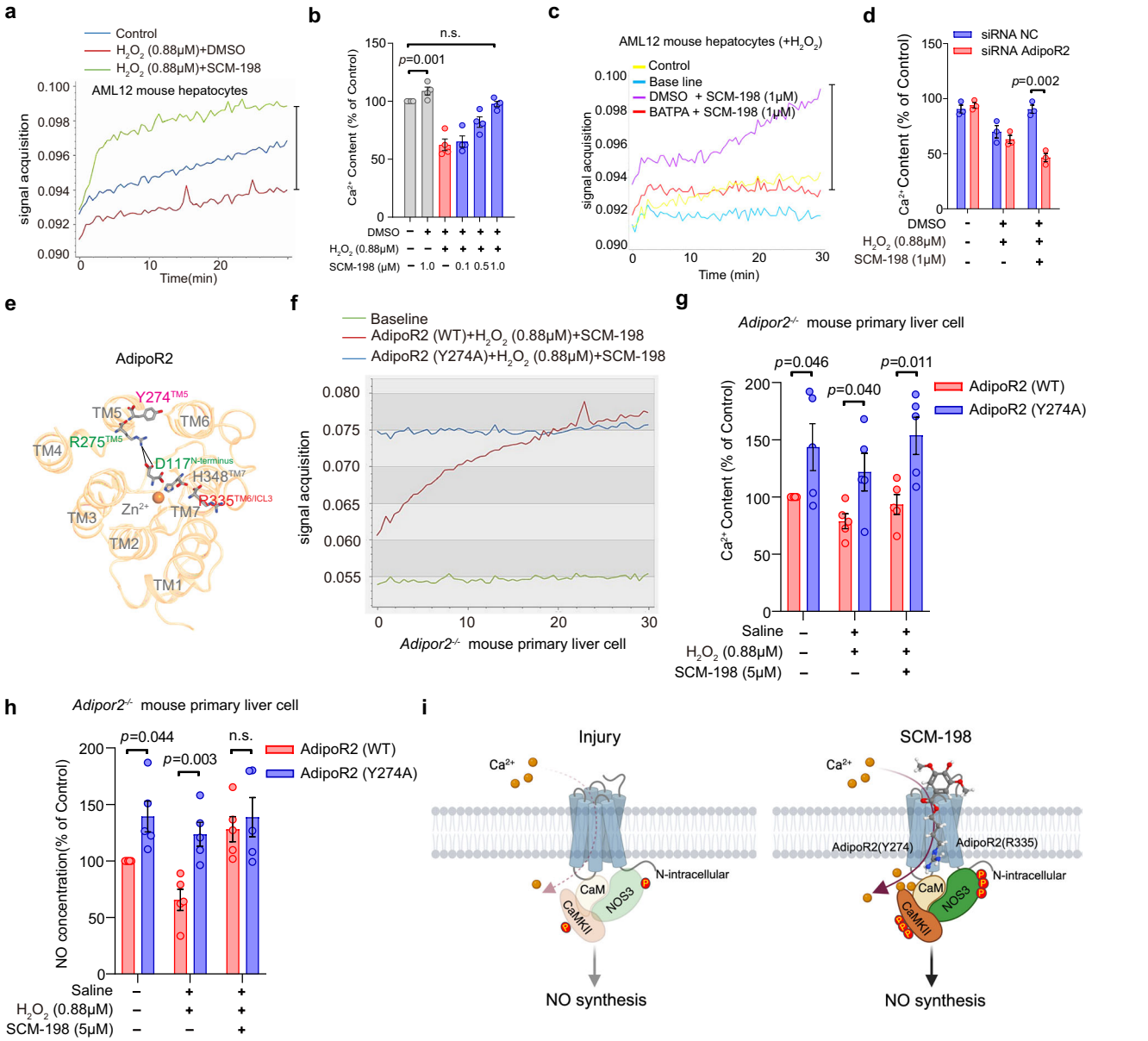


**Fig. 7 | SCM-198 induces $Ca^{2+}$ influx controlled by the Y274 residue of AdipoR2.** **a** Time-course dynamics of Flow-4 AM fluorescence in AML12 hepatocytes, treated with DMSO or SCM-198 following $H_2O_2$ exposure. **b** Quantification of intracellular $Ca^{2+}$ content in AML12 hepatocytes treated with DMSO or SCM-198 (0.1, 0.5, 1 μM) for 24 h after $H_2O_2$ exposure ($n = 4$ experimental repeats). **c** Dynamics of Flow-4 AM fluorescence in AML12 hepatocytes, treated with DMSO or SCM-198 following $H_2O_2$ exposure, with or without BATPA. **d** $Ca^{2+}$ quantitative assay for AML12 hepatocytes treated with SCM-198 after $H_2O_2$ exposure, with or without AdipoR2 knockdown ($n = 3$ experimental repeats). **e** Molecular docking analysis of $R275^{TM5}$-$D117^{N\text{-terminus}}$ interaction of ADIPOR2 (PDB ID: 6KS1), viewed from the intracellular side. The binding of $Y274^{TM5}$ by SCM-198 increases the hydrophobicity of $R275^{TM5}$, potentially leading to the opening of the internal cavity, allowing ion inflow. $R275^{TM5}$, $D117^{N\text{-terminus}}$, $H348^{TM7}$, and $R335^{TM6/ICL3}$ are shown as sticks. **f** Dynamics of Flow-4 AM fluorescence in *Adipor2*$^{-/-}$ mouse primary hepatocytes with overexpression of $AdipoR2^{WT}$or $AdipoR2^{Y274A}$, treated with SCM-198 after $H_2O_2$ exposure. **g**, **h** Quantification of intracellular $Ca^{2+}$ content (**g**) and NO concentration (**h**) in *Adipor2*$^{-/-}$ mouse primary hepatocytes with overexpression of $Adipo2^{WT}$or $AdipoR2^{Y274A}$, treated with SCM-198 after $H_2O_2$ exposure ($n = 5$ experimental repeats). **i** A model of actions of SCM-198. There exists an AdipoR2-CaM-CaMKII-NOS3 axis in liver cells. TAA/APAP or $H_2O_2$ injuries reduce phosphorylation levels of NOS3 and CaMKII. The binding of SCM-198 to AdipoR2 through R335 and Y274 causes $Ca^{2+}$ influx and increases phosphorylation levels of NOS3 and CaMKII, leading to quick upregulation of NO synthesis. Created in BioRender. Lin, G. (2024) https://BioRender.com/n69o964. Data in (**b**, **d**, **g**, **h**) are presented as mean ± SEM. The *p*-values were determined using SPSS v20 for *t test*, two-tail analysis. ns: not significant. Source data are provided as a Source Data file.

## Discussion

The pathogenesis of ALF involves multiple phases, including abnormal lipid accumulation and lipid peroxidation, uncontrolled sterile inflammation, and massive hepatocyte death[74–76]. When untreated, ALF continues even after the concentration of hepatotoxin has declined to unmeasurable levels. Inflammation mediators such as TNF-α from necrotic hepatocytes drive neutrophils chemotaxis and activate sterile inflammation, further exacerbating liver injury[77–79]. Thus, the earlier the intervention, the better the outcomes. However, treating ALF early is challenging since liver intoxications are often hard to be diagnosed early[12,80]. Our study demonstrates that the bioactive compound SCM-198 acts in multiple aspects of ALF pathogenesis. SCM-198 reduces the serum ALT and AST levels, mitigates abnormal lipid peroxidation, inhibits inflammation spreading, regulates lipid metabolism, and enables 100% survival of the animals (Figs. 1, 4, 5, 8 and Supplementary Figs. S1 and S8).

https://doi.org/10.1038/s41467-024-55295-7

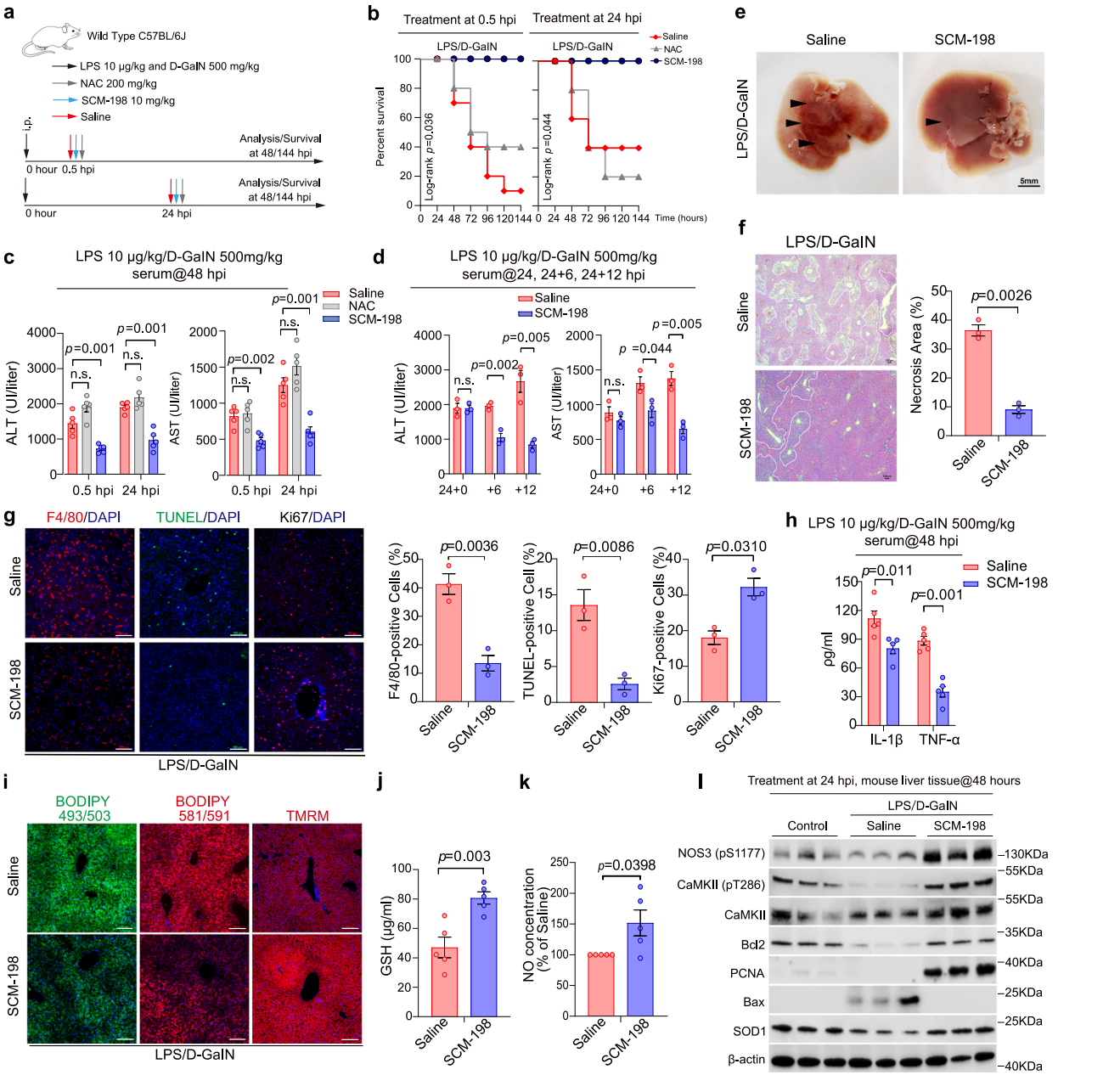


**Fig. 8 | Hepatoprotection by SCM-198 in LPS/D-GalN-induced ALF mice.** **a** Schematic diagram of the LPS/D-GalN-induced ALF model. **b** Percent survival chart of LPS/D-GalN-induced ALF mice after saline, NAC, or SCM-198 treatment given at 0.5 or 24 hpi ($n = 10$ per group). The $p$ values were determined using the Log-rank test. **c** Serum ALT and AST levels were measured at 48 hpi in LPS/D-GalN-induced ALF mice treated with saline, NAC, or SCM-198 ($n = 5$ mice). **d** Serum ALT and AST levels in LPS/D-GalN-induced ALF, at 24 + 0, 24 + 6, 24 + 12 h after SCM-198 administration. ($n = 3$ mice). **e** Representative photographs of LPS/D-GalN-induced ALF livers, 48 hpi. Black arrowheads indicate lesion areas. Scale bars, 5 mm. **f** Representative micrographs of HE staining on the section of LPS/D-GalN-induced ALF liver. Scale bars, 100 μm. Quantification analysis of necrosis areas on liver sections was from 3 animals. **g** Representative immunofluorescence images of F4/80 + cells, TUNEL + cells, or Ki67 + cells on liver sections, 48 hpi. Quantification analysis was performed on 3 animals. **h** Plasma levels of IL-1β and TNF-α detected by ELISA, 48 hpi ($n = 5$ mice). **i** Representative images of BODIPY 493/403, BODIPY 581/591, and TMRM staining on liver sections, 48 hpi. **j** Serum GSH levels detected by ELISA, 48 hpi ($n = 5$ mice). **k** Liver tissue NO content, relative to the saline-treated liver, 48 hpi ($n = 5$ mice). **l** Immunoblotting of NOS3(pS1177), CaMKII(pT285), SOD1, PCNA, Bcl2, Bax in LPS/D-GalN-induced ALF liver tissues. Mice were treated with saline or SCM-198 at 24 hpi, and samples were collected at 48 hpi. Similar results were obtained in 2 independent repeats. Data in (**c**, **d**, **f**–**h**, **j**, **k**) are presented as mean ± SEM. The $p$-values were determined using SPSS v20 for $t$ *test*, two-tail analysis. n.s., not significant. Source data are provided as a Source Data file.

More importantly, SCM-198 extends the time window for ALF treatment. In ALF animal models, most studies treat the animals at the early injury stages, before or immediately after drug administration[21,22,26,27]. This is because extensive liver damage has already occurred at the 2 h time point[27,29,81]. Thus, treatment after the first 3 h is less effective in attenuating liver injuries. In contrast, SCM-198 effectively extends the treating window from 2 hpi to at least 24 hpi in TAA-, APAP-, and LPS/D-GalN- induced murine ALF models (Figs. 1, 8 and Supplementary Figs. S1, S8). SCM-198 acts rapidly, even when used at 24 hpi in the murine ALF models, decreasing serum ALT and AST

https://doi.org/10.1038/s41467-024-55295-7

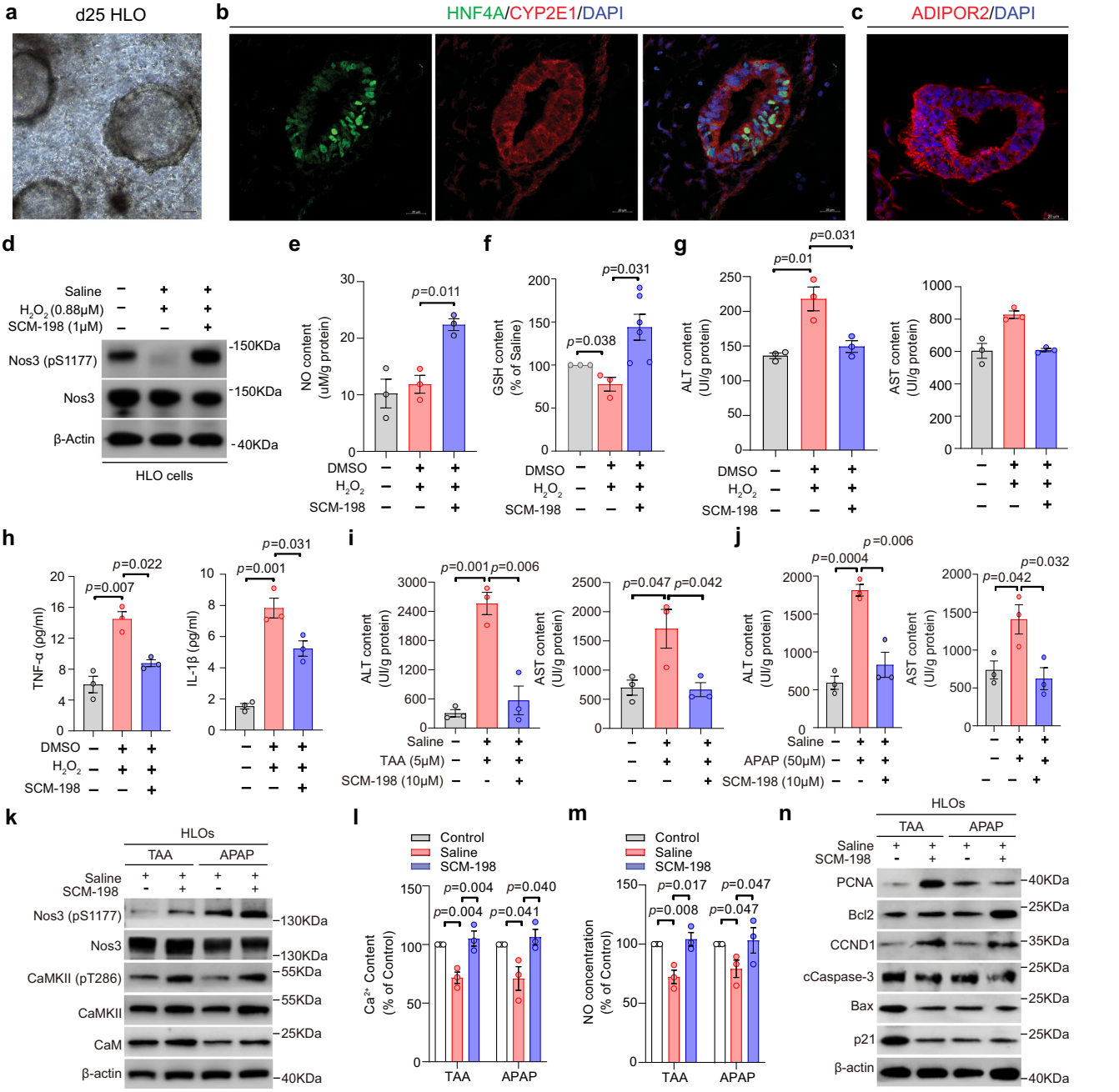


**Fig. 9 | SCM-198 alleviates oxidative stress and TAA/APAP injury in human liver organoids. a** Micrograph of human liver organoids (HLO) on day 25 (d25) of induction. **b**, **c** Immunofluorescence staining of HNF4A (green, **b**), CYP2E1 (red, **b**), ADIPOR2 (red, **c**) on sections of d25 HLO. Nuclei were counterstained with DAPI. Scale bar: 20 μm. **d** Immunoblotting of NOS3(pS1177) and NOS3 in HLOs, with saline or SCM-198 treatment after $H_2O_2$ exposure. β-actin as loading control. **e** NO content in HLOs treated with DMSO or SCM-198 after $H_2O_2$ exposure. Cellular NO contents were detected by Griess assays and normalized to protein content. **f** GSH levels of HLOs treated with DMSO or SCM-198 after $H_2O_2$ exposure. GSH content normalized to protein was compared to control HLO. **g** Contents of ALT and AST in HLO culture medium (UI/L) treated with DMSO or SCM-198 for 24 h following $H_2O_2$ exposure, normalized to protein content (g/L) of HLO lysis. **h** Levels of TNF-α, IL-1β, and TGF-β1 in medium of HLOs treated with DMSO or SCM-198 for 24 h following $H_2O_2$ exposure. **i**, **j** Contents of ALT and AST in the medium of HLO treated with or without SCM-198 for 24 h following TAA (**i**) or APAP (**j**) injury, normalized to protein content (g/L) of HLO lysis. **k** Immunoblotting of NOS3, NOS3(pS1177), CaMKII, CaMKII(pT286), and CaM in HLOs injured with TAA/APAP and treated with saline or SCM-198. β-actin as loading control. **l**, **m** Contents of $Ca^{2+}$ (**l**) and NO (**m**) in HLOs treated with saline or SCM-198 for 24 h following TAA or APAP injury, normalized to protein content. **n** Immunoblotting of PCNA, BCL2, CCND1, cCaspase-3, BAX, and P21 in HLOs Injured with TAA or APAP and treated with saline or SCM-198. Data in (**e**–**j**, **l**, **m**) are presented as mean ± SEM ($n = 3$, independent HLO batches). The *p*-values were determined using SPSS v20 for *t test*, two-tail analysis. Similar results were obtained in 3 (**a**–**d**), or 2 (**k**, **n**) independent experimental repeats. Source data are provided as a Source Data file.

levels within 6 h post-administration (Figs.1 and 8). Thus, SCM-198 is an effective therapy for established murine ALF.

Current ALF therapies include supportive care, N-acetylcysteine (NAC) for APAP overdose, corticosteroids for autoimmune hepatitis, artificial liver support devices, continuous renal replacement therapy (CRRT), and liver transplantation. NAC is safe, cost-effective, and highly effective in early treatment, significantly reducing mortality when administered within 8 h of APAP-induced liver injury[13–17]. However, its effectiveness drops significantly beyond this window, leading to higher mortality rates (~40%) in severe cases[13–17]. Liver assist devices,

such as the molecular adsorbent recirculating system (MARS), offer temporary stabilization but do not eliminate the need for liver transplantation. CRRT reduces deaths from refractory cerebral edema[82], but is costly and must be used early. For many advanced ALF patients, timely liver transplantation remains the only definitive treatment, but this is limited by the shortage of donors and high costs[16]. Emerging regenerative therapies also show promise in ALF treatment in preclinical animal models[32,83], but these procedures are expensive, time-consuming, and require immunosuppression if the cells are derived from donors. Overall, there is an unmet need for therapeutic strategies that combine detoxification with liver regeneration stimulation. Our study demonstrates that SCM-198 effectively extends the treatment window from 3 hpi to at least 24 hpi in murine ALF. As ALF progression is much faster in mice than in humans[11], SCM-198 could benefit advanced-stage ALF patients as either a curative therapy or a bridge to liver transplantation. Indeed, SCM-198 demonstrates efficacy in human liver organoid models of TAA and APAP injuries (Fig. 9). Given that SCM-198 has passed the safety test in clinical trials for hyperlipidemia treatment[34,36], selectively targeting AdipoR2 with SCM-198 may offer a low-cost and effective therapy for late ALF in humans.

Our identification of AdipoR2 as the specific binding partner of SCM-198 (Figs. 2 and 3) in the liver cells also solves the long-lasting question of the direct target of SCM-198. The formation of an AdipoR2-CaM-CaMKII-NOS3 complex provides a mechanistic explanation for SCM-198's rapid action (Fig. 6 and Supplementary Figs. S1 and S9). It is known that NOS3 activity is regulated by $Ca^{2+}$/Calmodulin (CaM) and CaMKII[62,63]. Thus, our study further extends the function of the $Ca2^{+}$/CaM/CaMKII-NOS3 complex by showing that AdipoR2 directly binds NOS3 in liver cells. This is the first time that direct interaction of AdipoR2 with NOS3 is found. This direct interaction allows rapid NO production.

Notably, SCM-198-induced NO production is independent of new protein synthesis (Fig. 7). This is consistent with our finding that the binding of SCM-198 to AdipoR2 induces $Ca^{2+}$ influx, enhances CaMKII and NOS3 phosphorylation and rapidly increases NO production (Fig. 7i). NO mediates SCM-198's hepatoprotective effect by reducing the production of inflammatory mediators (Figs. 1, 5) and inflammation spreading (Fig. 1g), and regulating fatty acid oxidation involving FA16:0 and FA18:00 (Supplementary Fig. S10), thus terminating lipid peroxidation[57]. The requirement for this complex for the hepatoprotection function of SCM-198 in ALF is demonstrated by the facts that loss-of-function of AdipoR2 or NOS3 both abolishes the protective effect of SCM-198 in TAA / APAP ALF mice (Figs.4, 5).

Our finding that SCM-198 selectively binds AdipoR2 but not AdipoR1 (Fig. 2) has significant implications in the study of adiponectin signaling, particularly when specific activation of AdipoR2 is desired, such as in distinguishing the roles of AdipoR2 versus AdipoR1 in stem cell pool regulation during aging[84]. Selective agonizts or antagonists for specific signaling receptors are highly desirable in drug discovery. For example, the thyroid hormone receptor beta–selective agonist Resmetirom is effective in treating NASH with liver fibrosis in a phase 3 clinical trial[85]. Resmetirom does not bind to TR-α, thereby avoiding the adverse effects associated with TR-α activation. In the case of Adiponectin signaling, uncontrolled activation of AdipoR1 leads to inhibition of the activity of the mitochondrial respiratory complex[86,87], which renders un-selective activation of adiponectin signaling unfavorable.

Moreover, our findings may guide the design of more potent AdipoR2 agonizts. MST and SPR data show that SCM-198 binds to AdipoR2 protein with a *Kd* of about 2 μM (Fig. 3). Although these values are within the range of intracellular concentrations of SCM-198 detected in mice or rhesus monkeys administered with regular doses[34,47,48], modifications of the SCM-198 molecule may further increase the affinity of SCM-198 to AdipoR2. Our results demonstrate that the R335 and Y274 residues of AdipoR2 are critical for AdipoR2 signaling after SCM-198 binding (Figs. 3, 6, and 7). Further cryo-EM study would provide more structural bases for the R335-SCM-198 interaction and address whether the structural difference between AdipoR2 and AdipoR1, as revealed in previous studies[66], accounts for the selectivity of binding of SCM-198 to AdipoR2.

A thorough understanding of the SCM-198-AdipoR2 signaling is essential for its translational application in ALF therapy. SCM-198 may bind to other proteins. For example, it was reported that SCM-198 could bind P3IK in liver lysates[88], although PI3K was not detected in our SCM-198 affinity pulldown analysis (Supplementary Table S1). Future work shall also investigate whether SCM-198-AdipoR2 signaling has a similar protective function in the repair and regeneration of other organs where AdipoR2 is expressed.

## Methods

This study was approved by the Institutional Animal Care and Use Committee (IACUC) of Tongji University (TJBC00422102) and the ethics committee of the Tongji Hospital affiliated with Tongji University (K-2024-066).

### Cell culture

AML12 (ATCC, CRL-2254), BNL CL.2 (ATCC TIB-73), and HEK293T (ATCC CRL-3216) cell lines were originally purchased from ATCC. AML12 hepatocytes were cultured in DMEM/F-12 supplemented with 10% Fetal Bovine Serum (FBS), 10 μg/ml insulin, 5.5 μg/ml transferrin, 5 ng/ml selenium, 40 ng/ml dexamethasone, 1% penicillin-streptomycin (PS), and 1% nonessential amino acids. BNL CL.2 and HEK293T cells were cultured in DMEM supplemented with 10% Fetal Bovine Serum (FBS), 1% penicillin-streptomycin (PS), and 1% non-essential amino acids. All cell lines used in this study were cultured in a humidified, 5% $CO_2$ air atmosphere at 37 °C.

### Generation of *AdipoR2* knockout AML12 cell line

To generate the *AdipoR2* knockout AML12 cell line, the GFP-2A-Neo-Stop sequence was inserted after the start codon of the first exon of *Aipor2* by using the CRISPR/Cas9 technology. The donor DNA fragment with *Adipor2* homologous arm of GFP-2A-Neo-Stop was amplified by PCR from the CSll-hMSI1-GFP-2A-Neo plasmid. 500 ng of Cas9 protein (Invitrogen), 125 ng of gRNA (Invitrogen), and 500 ng of donor DNA were transfected into a well of the 24-well plate for AML12 cells by using Lipofectamine CRISPRMAX Transfection Reagent (Invitrogen). After 48 h of transfection, G418 (Gibco, 20 μg/mL final concentration) was added to kill unsuccessfully homologous recombinant cells for one week. After G418 treatment, single cells were seeded into wells of a 96-well plate using the limited dilution method. After the monoclonal cells proliferated, a portion of the cells was scraped for genomic PCR to select homozygous monoclonal cells. The selected corresponding monoclonal cells were then expanded and cryopreserved. Deletion of AdipoR2 protein was confirmed by Immunoblotting.

### Animal husbandry

Male Wild-Type (WT) C57BL/6 J mice, 6-8 weeks old, were purchased from SLAC Laboratory Animal Company (Shanghai, China). *Adipor2*$^{-/-}$ (Cat. NO. NM-KO-190667), *NOS3*$^{-/-}$ (Cat. NO. NM-KO-18022) mice were obtained from Shanghai Model Organisms Center, Inc (Shanghai, China). Mice were housed in a specific pathogen-free (SPF) facility under standard conditions (22 ± 1 °C, 60% humidity, 12 h light-dark cycle with food and water ad libitum). Every effort was made to minimize pain and suffering and reduce the number of animals used in the study. All animal care and treatment procedures were performed following protocols approved by the Institutional Animal Care and Use Committee (IACUC) of Tongji University.

### Mouse ALF models

Mouse ALF models generated with APAP, TAA, or LPS/D-GalN have been described previously[20–27,29–33]. TAA (200 mg/Kg body weight),

APAP (400 mg/Kg body weight), or LPS (10 μg/kg)/D-GalN (500 mg/kg) was injected intraperitoneally into male adult C57BL/6 J mice. The dosages used in this study allowed the mice to survive at least 24 h after liver intoxication for testing the effect of NAC or SCM-198 treatment at 24hpi. Mice were monitored closely following hepatotoxicant injection, and the successful establishment of ALF models was determined based on behavioral changes (such as loss of appetite, lethargy, ataxia, and tremor) (for example, see Supplementary Movie 1) and elevated serum ALT and AST levels. The resumption of normal behavior, serum ALT/AST levels, and post-mortem histology and immunofluorescence analyses were used to assess the hepatoprotective effects of treatments. ALF mice were randomly grouped into saline, NAC, or SCM-198 groups. Saline, or NAC (200 mg/Kg), or SCM-198 (10 mg/Kg) was administered at 0.5 or 24 hpi. For survival rate analysis, mice were monitored until 144 hpi. For mechanism studies, mice were anesthetized with isoflurane at 48 hpi for blood collection and then euthanized by cervical dislocation for liver sample collections.

### Biochemical assay and histology

Both biochemical and histological assessments were used to determine liver injury. Mouse serum alanine aminotransferase (ALT), aspartate aminotransferase (AST), and total bilirubin (TBIL) levels were determined by a biochemical detector at Tongji Hospital Clinical Laboratory using commercial kits (listed in the Supplementary Data 2) according to the manufacturer's instructions. Mouse liver was harvested, fixed in 4% Paraformaldehyde (PFA), washed with PBS, and embedded in either paraffin (following dehydration with ethanol gradients) or O.C.T compound (following dehydration with 15% and 30% sucrose in PBS). Sections were cut with a Leica cryostat or microtome and rehydrated before hematoxylin-eosin staining, PAS staining, or subjected to immunofluorescence staining. For statistical analysis of necrosis, three sections randomly chosen from the liver tissues were imaged and analyzed with ImageJ. At least 3 animals were used in each group of experiments.

### Immunofluorescence staining

For immunofluorescence staining, liver sections or cells fixed by 4% PFA were permeabilized with 1% TritonX-100 in PBS and blocked with 5% BSA and 0.3% TritonX-100 in PBS. Samples were blocked with M.O.M. if mouse-sourced antibodies were used. The samples were then incubated with primary antibody overnight at 4°C. After washing with PBS, samples were incubated with Alexa Fluor 488 or Alexa Fluor 555-conjugated secondary antibodies for 60 min at 3 °C before counterstaining with DAPI. Sections were mounted using a Fluoro-Gel mounting medium (Electron Microscopy Sciences). The antibodies used are listed in Supplementary Data 2. In animal experiments, the liver samples were sectioned and stained. For statistical analysis, at least three sections from three positions of the liver were selected and counted. Liver sections from three individual animals were used. Human liver specimens used for ADOPOR2 expression were obtained from the department of pathology, originally obtained as paraneoplastic tissue after tumor resection surgery and liver puncture of patients diagnosed with APAP-intoxication. The use of human liver specimens was approved by the Ethics Committee of Tongji Hospital of Tongji University, with written informed consent obtained from all participants. Immunofluorescence data were captured using DMI-6000B or DM-250 microscopes equipped with digital cameras (Leica).

### EdU assay

AML12 mouse hepatocyte cells were seeded on a 6-well plate at 10,000 cells per well. At 48 h after seeding, cells were treated with 5 mM EdU (Share-Bio, or Thermo Fischer Scientific) for 4 h. Cells were washed twice with PBS and fixed with 3.7% formaldehyde in PBS. AML12 mouse hepatocytes were imaged following the application of standard fluorescence protocols of the EdU assay kit. Cells were counterstained with DAPI.

### TUNEL staining

A one-step TUNEL detection kit (Beyotime, China) was used according to the manufacturer's instructions. Briefly, the tissue sections were washed twice with PBS and incubated with 50 μL of TUNEL detection solution at 37 °C in a humid box for 60 min, followed by washing with PBS three times. The slides were mounted using an anti-fluorescence quenching sealing solution and observed under a fluorescence microscope (Leica DMI6000).

### TMRM, BODIPY 493/503 and BODIPY 581/591 staining

Cells or tissue sections were washed with PBS three times and incubated with TMRM, BODIPY 493/503 (1: 1000 dilution in PBS), or BODIPY 581/591 (1: 1000 dilution in PBS) at 4 °C overnight. Nuclei were counterstained with DAPI. The images were taken with a fluorescent microscope (Leica Sp5 Laser Scanning Confocal Microscope), and the fluorescence intensity was analyzed with ImageJ.

### GSH content detection

A CheKine™ Micro Reduced Glutathione (GSH) Assay Kit (Abbkine) was used for GSH content detection according to the manufacturer's instructions. About 0.1 g of liver tissue was homogenized in 1 mL of precooled extraction buffer, followed by centrifugation at 4 °C 8000 × *g* for 10 min for supernatant collection. The standard or supernatant was mixed with deionized water, Assay Buffer, and Chromogen, incubated at room temperature in the dark for 2 min and the absorbance at 412 nm was recorded. The GSH content was calculated from the standard curve and normalized to protein concentration quantified by a BAC protein assay kit (Thermo Fischer Scientific). For HLOs, cells were collected from a well of 24-well plate and extracted with 0.1 mL of extraction buffer.

### Label of Biotinylated SCM-198

A Biotin conjugation kit (Abbkine Scientific) was used to label SCM-198 with Biotin according to the manufacturer's instructions. Briefly, 100 μl of SCM-198 stock (2 mg/mL) was mixed with 15 μL Biotin labeling solution by pipetting, followed by adding 7.5 μL of activated Biotin solution and adding water to a final volume of 150 μl. The reaction mixture was kept dark at 37 °C for 1 h Then, 350 μl of PBS was added to the mix, which was transferred to the purification column and centrifuged at 4 °C and 12,000 × *g* for 10 min. The column was washed with 500 μl of PBS. The purification column was inverted into a collection tube and centrifuged at 4 °C and 4000 × *g* for 2 min to collect the labeled SCM-198-Biotin.

### Cell membrane protein and cytoplasmic protein extraction

Cell membrane protein and cytoplasmic protein were extracted using an extraction kit (Beyotime, China). For cells, 20-50 million cells were used. Cells were washed with PBS once, scraped off the culture surface with a cell scraper, and collected by brief centrifugation. To extract cell membrane and cytoplasmic protein from tissues, 100 mg of tissue was cut into small fragments with scissors and collected into a centrifuge tube. The cell pellet or tissue fragments were resuspended with 1 ml of membrane protein extraction reagent supplemented with PMSF and were kept in an ice bath for 15 min. The cell suspension or tissue samples were transferred to pre-cooled glass homogenizers and manually homogenized in an ice bath about 50 times. The samples were transferred into centrifuge tubes and centrifuged at 700 × *g* for 10 min at 4 °C. The supernatant was collected into a new centrifuge tube and centrifuged at 4 °C, 14,000 × *g* for 30 min. The supernatant was collected, this is the cytoplasmic fraction. The precipitate was resuspended with 100 microliters of membrane protein extraction reagent, with vortex and pipetting, and placed on ice for 5–10 min. The vortex and ice incubation steps were repeated 1-2 times to fully extract the membrane proteins. The resuspended samples were centrifuged at 4 °C, 14000 × g for 5 min, and the supernatant was

collected as the cell membrane protein solution, which was stored at − 80 °C for later use.

### Affinity purification pull-down assay

AML12 mouse hepatocytes cultured in 10 cm dishes were incubated with SCM-198-Biotin probe or Biotin (as controls) for 24 h. Cells were washed twice with cold PBS and then lysed in immunoprecipitation cell lysis buffer (Beyotime Biotech) supplemented with protease and phosphatase inhibitors (Thermo). After centrifugation at 12,000 × *g* for 15 min at 4 °C, the supernatant was collected and incubated with streptavidin-agarose beads for 24 h at 4 °C with rotation. The beads were washed three times with immunoprecipitation cell lysis buffer, and the bead-bound proteins were eluted for high-resolution peptide spectrometry or used for Immunoblotting.

For in vitro binding assay of purified recombinant human ADIPOR2 protein with SCM-198-Biotin probes, 1 μg of purified recombinant human ADIPOR2 were mixed with 10 μL of SCM-198-Biotin stock (final concentrations of 50 μM), incubated with streptavidin-magnetic beads for 24 h at 4 °C with rotation. The beads were washed three times with immunoprecipitation cell lysis buffer, and the bound proteins were eluted by elution buffer and separated by SDS-PAGE.

### High-resolution peptide spectrometry

SCM-198-bound proteins affinity purified from AML12 cell lysates was analyzed using a nano Elute (Bruker) coupled to a timsTOF Pro mass spectrometer (Bruker) equipped with a CaptiveSpray source. SCM-198-Biotin affinity-pulled recombinant ADIPOR2 protein from the in vitro binding assay was analyzed using a NanoLC 425 System (SCIEX) coupled to a TripleTOF 5600 + mass spectrometer (SCIEX).

**Sample preparation**. Following the procedure outlined in the affinity purification pull-down assay, the beads were washed with 1 mL of 50 mM ammonium bicarbonate (NH4HCO3) buffer. After centrifugation at 1000 rpm for 2 min, the supernatant was discarded. The sample was then reduced with 2 μL of 0.5 M Tris (2-carboxyethyl) phosphine (TCEP) at 37 °C for 60 min, followed by alkylation with 4 μL of 1 M iodoacetamide (IAM) at room temperature for 40 min in the dark. To precipitate the protein, five volumes of cold acetone were added, and the mixture was stored at − 20 °C overnight. After centrifugation at 12,000 × *g* for 20 min at 4 °C, the pellet was washed twice with 1 mL of pre-chilled 90% acetone aqueous solution and re-suspended in 100 μL of 100 mM triethylammonium bicarbonate (TEAB) buffer.

**Enzymatic digestion**. Based on molecular docking results predicting binding sites on either arginine (R) or tyrosine (Y), Trypsin was not used. Instead, Lysyl Endopeptidase (Sigma-Aldrich: A3547), which specifically cleaves at the carboxyl terminus of lysine (K), was employed. The enzyme was added at a ratio of 1:50 to protein mass and incubated at 37 °C overnight. The resulting peptide mixture was desalted using Pierce C18 Spin Tips and then concentrated in a speed vacuum concentrator.

**Mass spectrometry analysis**. The Ultimate 3000 (Thermo Fisher Scientific, MA, USA) liquid chromatography system was coupled to either the timsTOF Pro (Bruker) or the TripleTOF 5600 + mass spectrometer (SCIEX). Samples were reconstituted in 0.1% formic acid (v/v), and 200 ng of the peptide was separated using an AUR3-15075C18 column (15 cm length, 75 μm i.d, 1.7 μm particle size, 120 Å pore size, IonOpticks) with a 30 min gradient starting at 4% buffer B (80% ACN with 0.1% FA). The gradient increased stepwise to 28% in 15 min, 44% in 4 min, and 90% in 4 min, followed by a 3 min hold before re-equilibration at 4% for 4 min. The column flow rate was maintained at 400 nL/min with a column temperature of 50 °C.

Mass spectrometry data from samples of the recombinant ADIPOR2 protein were collected using the timsTOF Pro in PASEF mode and analyzed with Peaks Studio software (Bioinformatics Solutions). For samples from AML12 cell lysates, data were collected using the TripleTOF 5600 + mass spectrometer and analyzed with ProteinPilot software (v.5.0, SCIEX). The UniProt Reference Proteome database for mice or humans was utilized for data analysis.

### Verification of SCM-198-AdipoR2 binding and identification of binding sites on AdipoR2

For validation of the binding between SCM-198 and AdipoR2, the purified cytoplasmic and cell membrane proteins were prepared from a 10 cm dish of HEK293T cells (grown to 80% confluence) transfected with the pcDNA3-*Adipor2* plasmid (10 μg per dish for 24 h), incubated with SCM-198-Biotin and captured by streptavidin magnetic beads, then subjected to immunoblotting or LC-MS/MS analysis for the identification of modifications on the residues of AdipoR2.

### NO Fluorescent staining

The NO fluorescent staining kit (Beyotime, China) was applied for NO fluorescent staining according to the manufacturer's instructions. Briefly, the NO probe (DAF-FM DA) was diluted to 5 μM, added to the cells, and incubated at 37 °C for 20 min. After incubation, the cells were washed three times with PBS, and fluorescence was detected at 495 nm excitation and 515 nm emission by a plate reader (MULTISKAH SkyHigh, Thermo Fischer Scientific) or recorded under a fluorescence microscope (Leica DMI6000). For short stimulation (less than 2 h), the probe was loaded before stimulation. For long stimulation (more than 6 h), the probe was loaded after the cells were stimulated with 0.88 μM hydrogen peroxide supplement with or without SCM-198.

### Inflammatory factors and nitric oxide (NO) content analysis

ELISA kits were used to detect the levels of TNF-α, IL-1β, and HMGB1 according to the manufacturer's instructions (listed in Supplementary Data 2). The NO content in cell lines or liver tissue was quantified using a Nitric Oxide Assay Kit (Share-bio, China) via Griess reaction. Briefly, cells were washed with PBS, precipitated by centrifugation at 4 °C 500 × *g* for 5 min, lysed by freeze-thaw cycle, and centrifuged to obtain the supernatant. The supernatant was diluted to 50 μL by 0.9% NaCl for analysis following the manufacturer's instructions. Samples and standards were assayed in triplicates on 96-well plates, with the absorbance at 540 nm recorded by a plate reader (MULTISKAH SkyHigh, Thermo Fischer Scientific). NO content was calculated based on the standard curve and normalized by each diluted supernatant protein concentration quantified by a BAC protein assay kit (Thermo Fischer Scientific). Cells were collected from 3 independent batches of cultures. For liver tissues, 0.1 g of tissues were homogenized in 0.1 mL of RIPA buffer before being subjected to the protocols described above.

### Immunoprecipitation

For immunoprecipitation with hepatocytes, $1 \times 10^7$ cells were washed three times with pre-chilled PBS and resuspended in 2 ml of PBS. The cells were harvested by centrifugation and washed twice with ice-chilled PBS. Cells were resuspended in 2 ml of immunoprecipitation lysate buffer containing protease inhibitors. Insoluble material was removed by centrifugation at 16,000 × *g* for 10 min at 4 °C. The supernatant was mixed with the antibody and incubated overnight at 4 °C with rotation, followed by incubation with protein A/G beads. Isotype IgG antibodies were used as controls. The beads were collected by centrifugation at 6000 rpm for 30 s and washed five times with wash buffer (50 mM Tris-Cl, pH 7.5, 1% NP-40, 1% sodium deoxycholate, 0.1% SDS, 1 mM EDTA, 1 M NaCl, and 0.2 mM PMSF). The beads containing the immunoprecipitated samples were collected and resuspended in resuspension buffer (50 mM Tris-Cl, pH 7.0, 5 mM EDTA, 10 mM DTT, and 1% SDS) and incubated at 100 °C, 10 min for separation and denaturation. The immunoprecipitated proteins were used

for subsequent Immunoblotting analysis. For liver tissues: 0.1 g of liver tissues were homogenized with immunoprecipitation lysate buffer.

### Immunoblotting

Cells or liver tissues were collected and homogenized with RIPA buffer (Thermo Fischer Scientific) containing complete protease inhibitors for protein extraction. Cytoplasmic fractions of the proteins were used for subsequent analysis. For nuclear and cytoplasmic fractionation, the Qproteome Nuclear Protein Kit (QIAGEN) was used. The protein concentration was quantified by a BAC protein assay kit (Thermo Fischer Scientific). Cell Lysate was denatured by adding 6 × sample buffer containing 330 mM Tris-Cl pH 6.8, 30% glycerol,1 mM EDTA, 9 % sodium dodecyl sulfate (SDS), 550 mM DTT, 0.3% bromophenol blue and heated for 10 min at 90 °C. Proteins were separated on SDS-polyacrylamide gels and processed for conventional western blotting. The primary and secondary antibodies were diluted in TBST (Tris: 20 mM, NaCl: 150 mM, Tween® 20 detergent: 0.1% w/v) containing 5% (w/v) skimmed milk. Peroxidase activity was detected by chemiluminescence (Tanon, High-sig ECL Western Blotting Substrate, Cat#180-501) and captured with Amersham Imager 600 (General Electric). The antibodies used are listed in Supplementary Data 2.

### ADIPOR2 protein expression and purification

His-tagged ADIPOR2 was expressed in suspension HEK293T cells by Cusabio (Wuhan, China). Briefly, a total of 200 ml cells at $5 \times 10^6$ per ml (with viability higher than 90%, as determined by Trypan Blue staining) were transfected with 200 μg of each plasmid dissolved in 2 ml of SMM 293-T II medium containing 1500 μg of PEI. After 48 h, cells were collected by centrifugation at 2000 × *g* and then lysed with 100 mL of ice-cold lysis buffer. The lysates were then sonicated and centrifuged at 20,000 × *g* for another 30 min at 4 °C. Anti-His Affinity beads (1:100, balanced in lysis buffer) were added into the supernatant and mixed for 4 h at 4 °C. The beads were washed with 200 times the volume of lysis buffer 3 times at 4 °C. Proteins were then eluted with 1 ml of His tag peptide (400 μg $mL^{-1}$ Final concentration: 1.0 or 2.5 mM concentration) for another 1 h at 4 °C. Eluent was diluted with 15 mL of PBS buffer, then concentrated to 1 mL using an Amicon Ultra-15 centrifugal filter unit with Ultracel-10 regenerated cellulose membrane. Such a process for buffer exchange was performed another two times before experiments. It's important to note that experiments involving proteins expressed and purified described above should be performed on the same day after purification to avoid freeze-thaw cycles.

### Molecular docking

The potential binding sites on the AdipoR2 were detected using the fpocket program. The predicted five top-ranked binding sites were selected for docking studies. Molecular docking of SCM-198 to the five binding sites of AdipoR2 was performed using the AutoDock 4.2 program. Polar hydrogen atoms were added to the AdipoR2. Kollman united partial atomic charges were then assigned, and the AutoDock atom types were defined for the protein using AutoDock Tools (ADT). Gasteiger charges were added to SCM-198 with the default root, rotatable bonds, and torsion setting using the TORSDOF module in ADT. The grid center was defined at the centroid of the five binding sites, and the numbers of grid points in the x, y, and z directions were set to 60, 60, and 60 with a spacing value of 0.375 Å. The Lamarckian genetic algorithm was used for the SCM-198 conformational search with identical docking parameters used in our previous protocols. Fifty independent docking runs were conducted, and the binding energy was used to rank the docked SCM-198 in order of fitness.

### Surface plasmon resonance (SPR)

Experiments were performed in triplicate at 25 °C on a BIAcore T200 using CM5 sensor chips, and data were analyzed using BIAcore T200 Evaluation software (GE Healthcare) following the manufacturer's instructions. In brief, a cell on the CM5 sensor chip was activated with a mixture of 200 μM 1-Ethyl-3- [3-dimethylaminopropyl] carbodiimide hydrochloride (EDC) and 50 μM N-hydroxysuccinimide (NHS) at 10 μL $min^{-1}$ for 10 min. A total of 20 μL of AdipoR2 protein (1 μg $\mu L^{-1}$) purified as described above and adjusted to pH 4.0 (by mixing with 180 μL of 10 mM sodium acetate solution, pH 4.0) was then immobilized on the surface of the cell at 10 μL $min^{-1}$ for 5 min for two repetitive runs. The cell was then blocked with 1 M Ethanolamine (10 μL $min^{-1}$ for 10 min). SCM-198 stock solution (1 mM) was diluted to a series of concentrations (50.00, 25.00, 12.50, 0.79, 0.39, and 0.20 μM (all in PBS)) and was flowed at 30 μL $min^{-1}$ for 150 s in each run. At the end of each flow, proteins were regenerated for 5 min with 10 mM glycine-HCl (pH 2.0) solution at 10 μL $min^{-1}$. Data from the sample protein were collected using BIAcore T200 Control software (v. 2.0, GE Healthcare) from the reference protein. The association and dissociation constants were calculated using a global fit data fit to a 1:1 binding model using BIAcore T200 Evaluation software (v.2.0, GE Healthcare). The data was exported to generate the final figures.

### Differential scanning calorimetry (DSF)

Differential scanning calorimetry assays were performed on a VP-DSC (GE Healthcare). The VP-DSC was run on a mode without feedback, and 15 min of equilibration at 20 °C was performed before and between each scan. The scanning range was set from 20 to 80 °C, and the heating rate was 90 °C $h^{-1}$. The instrument was pre-equilibrated by running for five heating-cooling cycles with both the sample cell and the reference cell loaded with PBS. The sample cell was then loaded with 10 μL of AdipoR2 protein at 1 μg $\mu L^{-1}$ in 10 μM SCM-198 (in DMSO), or DMSO control, and curves of heat capacity (Cp) versus temperature were recorded. Data were collected using VPViewer 2000 software (v2.66.7, GE Healthcare) corrected for PBS baselines, and normalized for scan rate and protein concentration.

### Microscale thermophoresis (MST)

To determine the binding affinity of SCM-198 and ADIPOR2, an MST assay was conducted. Monolith NT.115 (NanoTemper Technologies) was used. ADIPOR2 was labeled with the Monolith NT™ Protein Labeling Kit RED (NanoTemper Technologies) according to the supplied labeling protocol. Labeled AdipoR2 was used at a concentration of ~ 20 nM. SCM-198 was titrated in 1:1 dilutions beginning at 25 μM, which contained 1.25% (v/v) DMSO. The samples were diluted in a MAT assay buffer. The mixture consisted of 100 mM Tris-HCl pH 8.0, 20 mM $MgCl_2$, and 200 mM KCl. DMSO should be at a final concentration of 1.25% to guarantee accuracy. All samples have the same DMSO concentration. The pieces were filled into premium-coated capillaries for measurement.

### DNA Constructs, point-mutation and delivery method

DNA constructs used in this work were prepared by PCR amplification of target genes from the cDNA of mouse liver and cloned into pcDNA3 vectors for over-expression. Flag tags and restriction enzyme sites were added to the DNA constructs during PCR amplification. The over-expression vectors were delivered into cells by Lipofectamine 3000, and expression was confirmed by immunofluorescence staining or western blotting. Point mutation constructs of AdipoR2 were generated with point-mutation primers (listed in Supplementary Data 2) with a point mutation PCR kit (Sigma). The mutation was verified by DNA sequencing.

### RT-PCR and RT-qPCR

Total RNA was extracted using Trizol reagent (Life Technologies), treated with Turbo DNase I (Ambion), and reverse-transcribed into complementary DNA using the Superscript IV RT system (Life Technologies). GoTaq® G2 Master Mixes (Promega) were used for RT-PCR. RT-PCR primers are listed in Supplementary Data 2. For RT-qPCR, the

TransScript® Uni All-in-One First-Strand cDNA Synthesis SuperMix for qPCR kit (TransGen) was used for cDNA synthesis. SYBR Green PCR Master Mix was used for RT-qPCR and detection using Light-cycler (Roche).

### siRNA interference transfection

Custom and chemically modified small interfering RNA (siRNA) was designed to target mouse *Adipor2* (GenePharma). Non-specific siRNA duplex served as control (GenePharma). To knock down *Adipor2* in vitro, AML12 mouse hepatocytes cultured in 6 cm dishes were transfected with 30 pmol of siRNA with 3 μL of the Lipofectamine® 2000 Reagent (Thermo Fisher). Cells were collected 48 hours after transfection. Sequences of the *Adipor2* siRNA were: R2-381, 5′-CGA-GUGUCAUGAUGACAAUTT-3′; R2-922, 5′-CCACAACCUUGCUUCAU-CUTT-3′; R2-1207, 5′-CCUGGCAAAUGUGACAUCUTT-3′. A similar efficiency of AdipoR2 knockdown was obtained with all three siRNAs. The results shown were obtained with siRNA R2-381.

### Targeted lipidomics

Total lipid was extracted from $2 \times 10^7$ cells using the modified method of Bligh and Dyer. An internal standard cocktail (Avanti Lipids Polar) was added at 10 μL to each sample according to 1 mg of extracted tissue protein during lipid extraction. Lipid extracts were subjected to triple-quadrupole MS (QTRAP 4000 and 6500; SCIEX, MA). Both negative and positive electrospray ionization modes were used, and precursor ion scans and neutral loss scans were run in each mode. Lipid identification was based on MS data and assisted by the bioinformatics tool Lipid MS Predict (http://www.lipidmaps.org/). Quantitation was done by one internal standard per lipid class. Each experiment was repeated at least three times. Lipid compositions were separated on the Shimadzu LC-20AB HPLC system (Tokyo, Japan).

### Cell counting Kit-8 assay

A cell counting kit-8 (CCK8) was used according to the manufacturer's instructions. Briefly, 2000 cells were seeded into each well of a 96-well plate, with 200 μL of culture medium per well. After 24 h of seeding, the cells were treated with 0.88 μM $H_2O_2$ in the culture medium supplemented with or without SCM-198 for 24 h. Cells were washed three times with PBS and incubated in the culture medium supplemented with CCK-8 solution (1:10 dilution of the CCK-8 solution) for 2 h (the well without cell as blank control), and the absorbance at 450 nm was recorded by a plate reader (MULTISKAH SkyHigh, Thermo Fischer Scientific).

### Fluo-4 AM intensity measurement

Cells were digested with 0.05% (v/v) trypsin (without phenol red) and centrifuged at 500 g for 3 min, then resuspended and washed three times with PBS. Cells were resuspended and fixed for 5 min by adding 1 mL of 4% PFA. The fixation was terminated by adding 1 mL of 500 mM glycine in PBS and centrifuged at 500 × *g* for 15 min. 1:1000 dilution of Fluo-4 AM in PBS buffer was added, and the resuspended cells were incubated at 37 °C for 2 h. The cells were shaken gently several times during incubation. At the end of incubation, cells were centrifuged at 500 × *g* for 5 min, then resuspended in PBS and washed 3 times. Cells were resuspended in PBS for flow cytometry. Histograms of Fluo-4 AM fluorescence were analyzed with Flowjo 10 (BD Biosciences).

### Calcium content analysis

Quantitative calcium content assays were conducted in vitro with a Calcium Colorimetric Assay Kit (Beyotime Biotech) according to the manufacturer's instructions. Briefly, cells were washed with PBS and lysed with 200 μl of lysate buffer. Samples and standards were assayed in 96-well assay plates. 50 μL of samples or standards were mixed with 15 μL of detection buffer and 15 μL of developing bath, incubated at 37 °C for 30 min, and the absorbance at 450 nm was measured by a plate reader (MULTISKAH SkyHigh, Thermo Fischer Scientific). Calcium content was calculated based on the standard curve and normalized to protein concentrations detected by the BCA protein quantification kit (Thermo Fisher Scientific). Cells were collected from 3 batches of cultures independently.

### Calcium kinetic monitor

Fluo-4 AM probe was used for the calcium kinetic monitoring. About 10,000 cells/well were seeded in the 24-well black plate. After 24 h of seeding, 100 μl of Fluo-4 AM solution (diluted at 1: 1000) supplemented with 0.88 μM hydrogen peroxide and SCM-198 or without SCM-198 were added into the well and incubated at 37 °C for 15 min. After incubation, the fluorescence intensities were detected at 510 nm with a full-band microplate reader (Thermo Fisher Scientific). The intensities at $t = 0$ as a baseline and the intensities were continuously monitored for 30 min.

### RNA-sequencing and analysis

Liver tissue was collected at 48 hpi from mice treated with SCM-198 or saline at 24 hpi. Total RNA was extracted using the TRIzol reagent (Invitrogen, CA, USA) according to the manufacturer's instructions. RNA purity and quantification were evaluated using the NanoDrop 2000 spectrophotometer (Thermo Scientific, USA). RNA integrity was assessed using the Agilent 2100 Bioanalyzer (Agilent Technologies, Santa Clara, CA, USA). Libraries were constructed using the VAHTS Universal V6 RNA-seq Library Prep Kit according to the manufacturer's instructions. The transcriptome sequencing and analysis were conducted by OE Biotech Co., Ltd. (Shanghai, China). The libraries were sequenced on the Illumina Novaseq 6000 platform, and 150 bp paired-end reads were generated. The low-quality reads were removed to obtain the clean reads using fastp[89]. The clean reads were mapped to the mouse genome (mm10) using HISAT2[90]. FPKM of each gene was calculated by HTSeq-count[91]. The R statistical package edgeR (Empirical Analysis of Digital Gene Expression in R)[92] was used for differential expression analysis. The DEGs between the two samples were selected using the following criteria: the logarithmic fold change was greater than 2, and the false discovery rate (FDR) should be less than 0.05. Panther was applied for GO enrichment analysis. Fisher's exact test was used for enrichment tests.

### Primary mouse hepatocyte isolation

The isolation and culture of mouse primary hepatocytes were performed as previously described[93]. The mouse was anesthetized and positioned on the dissection tray. The perfusion buffer and Liberase solution were warmed to 42 °C in a water bath. The tubing was primed with warm perfusion buffer (pump speed 3 mL/min). The mouse was secured on the edge of the dissection tray, and the fur was cleaned thoroughly with 70% ethanol. A "U"-shaped incision was made through the skin, and the separated skin was secured near the head using a needle. The intestine was moved to the right to reveal the portal vein and vena cava. With the pump turned on and warm perfusion buffer reached the needle (the buffer within the tubing has already cooled down to 20 °C–25 °C), the needle was inserted into the vena cava above the kidney. Immediately upon the appearance of white spots and/or portal vein swelling (occurs 3 s after cannulation), the portal vein was cut with scissors. After being perfused with perfusion buffer to remove blood from the liver, the portal vein was clamped with forceps and perfused the liver with pre-warmed Liberase buffer to digest the liver. The portal vein was clamped every minute but no more than 3 times during the Liberase buffer perfusion process. The liver was gently dissected and transferred to a 10 cm plate (not pre-coated with collagen) and ruptured to release the cell into the media. The cells were filtered through a 70 mm cell strainer into a 50 mL tube and collected by spinning at 50 x g for 2 min at 4 °C. Cells were resuspended with 10 mL of plating medium and washed with 10 mL Percoll

solution. Cells were spined at 200 x g for 10 min at 4 °C and resuspended and washed. The hepatocytes were counted and plated on collagen-coated cell culture plates/wells and cultured in a humidified $CO_2$ incubator for 16–20 h.

### Human liver organoids induction, treatment, and analysis

For human liver organoids (HLOs) induction, the first step was the definitive induction of endodermal differentiation, using the previously reported induction of differentiation method with slight modifications[71]. H9 hESCs (WiCell WA09) were cultured in mTeSR1 medium (StemCell Technologies) on plates coated with Matrigel (Corning). When cell colonies reached 80% confluence medium was changed to RPMI 1640 medium (Gibco) supplemented with Glutamax (Gibco) containing 100 ng/mL Activin A (Proteintech) and 50 ng/mL BMP4 (Proteintech) at day 1, supplemented with 100 ng/mL Activin A and 0.2% FBS (Gibco) at day 2, and supplemented with 100 ng/mL Activin A and 2% FBS at day 3. On Day4-6, the medium was switched to Advanced DMEM/F12 (Gibco) supplemented with B27 (Gibco) and N2 (Gibco) with 500 ng/mL FGF4 (Proteintech) and 3 μM CHIR99021 (Selleck). Spheroids appeared on the plate at day 6 of differentiation and were ready for HLO induction, using methods previously reported[69–72]. Briefly, cells were suspended by gently pipetting and centrifugation at 800 rpm for 3 min, and the supernatant was aspirated and resuspended on ice with 100% Matrigel and dropped on a cell culture dish and placed in a 37 °C cell incubator for 10 min to allow Matrigel to solidify. Cells were cultured in Advanced DMEM/F12 with B27, N2, and 2 μM retinoic acid (Sigma) for 4 days. Then, the medium was switched to Hepatocyte Culture Medium (Lonza) with 10 ng/mL hepatocyte growth factor (Proteintech), 0.1 μM Dexamethasone (Sigma), and 20 ng/mL Oncostatin M (Proteintech). Cultures for HLO induction were maintained at 37 °C in 5% $CO_2$ with 95% air and the medium was replaced every 3 days. To analyze HLO (day 25), organoids were isolated from Matrigel by scratching and pipetting.

For the TAA or APAP challenge, 5 μM TAA or 50 μM APAP, together with 10 μM SCM-198 or saline were added to the HLO culture, and the HLOs were collected for analysis 24 h later.

To detect ALT and AST in the supernatant of HLOs after $H_2O_2$ exposure, 20 μL of matrix solution was added to the measuring hole and the control hole, respectively, and then 5 uL of HLO supernatant was added to the measuring hole and incubated at 37 °C for 30 min. After incubation, 20 μL of 2,4 dimethylphenylhydrazine solution was added to the measuring hole and the control hole, respectively, and then 5 μL of the HLO supernatant was added to the control hole and incubated at 37 °C for 30 min. Then 200 μL of sodium hydroxide solution (0.4 mol/L) was added and incubated at room temperature for 15 min. The absorbance was measured at 510 nm wavelength. ALT and AST activity units were calculated from the standard curve and normalized to the protein amount of HLOs, and the results were presented in UI/g proteins. Three independent batches of HLOs were used.

To detect NO content in the HLOs, quantitative NO assays were conducted with Nitric Oxide Assay Kit (Beyotime Biotech) according to the manufacturer's instructions. Briefly, HLOs were collected by centrifugation (500 × *g*, 5 min, 4 °C), lysed by freeze-thaw cycles, and centrifuged to obtain the supernatant. The supernatant was diluted to 50 μL by 0.9% NaCl for analysis. Supernatants or standards were added into the assay plate wells and incubated with 150 μL of Griess Reagent mixture in the dark for 30 min. The absorbance at 540 nm was recorded by a plate reader (MULTISKAH SkyHigh, Thermo Fischer Scientific). NO content was calculated based on the standard curve and normalized by each diluted supernatant protein concentration quantified by a BCA protein assay kit (Thermo Fischer Scientific).

### Quantification and statistical analysis

Cells were observed under a Leica DM16FC or DMI6000 microscope or Leica Sp5 laser scanning confocal microscope. Images were taken with digital cameras (Leica) and analyzed by ImageJ. Figures were prepared with Adobe Photoshop and Illustrator (Adobe). Unpaired *t*-tests were used for the comparison of means of data between groups. Experimental data are presented as mean ± SEM. Statistical analyses were performed by using Prism GraphPad version 7.0 and SPSS version 22.0. Data normality was determined using the Histogram and Shapiro-Wilk tests. For comparison between the two groups, normally distributed data was analyzed by the Student *t* test; otherwise, data was analyzed by the Mann-Whitney U test. For comparison between multiple groups, One-way ANOVA with Tukey's test was generally applied. The survival curve was analyzed by a Log-rank (Mantel-Cox) test. Statistical significance was considered as $p < 0.05$.

### Reporting summary

Further information on research design is available in the Nature Portfolio Reporting Summary linked to this article.

## Data availability

RNA-seq data have been deposited at GEO with accession number GSE240824 and are publicly available as of the date of publication. LC-MS data supporting the findings of this study has been deposited at ProteomeXchange with ID PXD053870. All data supporting the findings described in this manuscript are available in the article and in the Supplementary Information and from the corresponding author upon request. Source data are provided in this paper.

## References

1. Stravitz, R. T. & Lee, W. M. Acute liver failure. *Lancet* **394**, 869–881 (2019).
2. Maiwall, R., Kulkarni, A. V., Arab, J. P. & Piano, S. Acute liver failure. *Lancet* **404**, 789–802 (2024).
3. Bernal, W. & Wendon, J. Acute liver failure. *N. Engl. J. Med.* **369**, 2525–2534 (2013).
4. Ostapowicz, G. et al. Results of a prospective study of acute liver failure at 17 tertiary care centers in the United States. *Ann. Intern. Med.* **137**, 947–954 (2002).
5. Serper, M. et al. Risk factors, clinical presentation, and outcomes in overdose with acetaminophen alone or with combination products: Results from the acute liver failure study group. *J. Clin. Gastroenterol.* **50**, 85–91 (2016).
6. Devarbhavi, H. et al. Global burden of liver disease: 2023 update. *J. Hepatol.* **79**, 516–537 (2023).
7. Shen, T. et al. Incidence and etiology of drug-induced liver injury in mainland China. *Gastroenterology* **156**, 2230–2241 (2019).
8. Hinson, J. A., Roberts, D. W. & James, L. P. in *Adverse Drug Reactions*. (ed. J. Uetrecht) 369–405 (Springer Berlin Heidelberg, Berlin, Heidelberg, 2010).
9. Jaeschke, H., Williams, C. D., Ramachandran, A. & Bajt, M. L. Acetaminophen hepatotoxicity and repair: the role of sterile inflammation and innate immunity. *Liver Int.* **32**, 8–20 (2012).
10. Yan, M., Huo, Y., Yin, S. & Hu, H. Mechanisms of acetaminophen-induced liver injury and its implications for therapeutic interventions. *Redox Biol.* **17**, 274–283 (2018).
11. Jaeschke, H., Xie, Y. & McGill, M. R. Acetaminophen-induced liver injury: From animal models to humans. *J. Clin. Transl. Hepatol.* **2**, 153–161 (2014).
12. Devarbhavi, H. et al. Drug-induced liver injury: Asia Pacific association of study of liver consensus guidelines. *Hepatol. Int.* **15**, 258–282 (2021).
13. Prescott, L. F. et al. Intravenous N-acetylcystine: the treatment of choice for paracetamol poisoning. *Br. Med. J.* **2**, 1097–1100 (1979).
14. Yip, L. & Dart, R. C. A 20-hour treatment for acute acetaminophen overdose. *N. Engl. J. Med.* **348**, 2471–2472 (2003).
15. Heard, K. J. Acetylcysteine for acetaminophen poisoning. *N. Engl. J. Med.* **359**, 285–292 (2008).

16. Whyte, A. J., Kehrl, T., Brooks, D. E., Katz, K. D. & Sokolowski, D. Safety and effectiveness of acetadote for acetaminophen toxicity. *J. Emerg. Med.* **39**, 607–611 (2010).
17. Bateman, D. N., Dart, R. C., Dear, J. W., Prescott, L. F. & Rumack, B. H. Fifty years of paracetamol (acetaminophen) poisoning: the development of risk assessment and treatment 1973–2023 with particular focus on contributions published from Edinburgh and Denver. *Clin. Toxicol.* **61**, 1020–1031 (2023).
18. Raghu, G. et al. The multifaceted therapeutic role of N-acetylcysteine (NAC) in disorders characterized by oxidative stress. *Curr. Neuropharmacol.* **19**, 1202–1224 (2021).
19. Knight, T. R., Ho, Y.-S., Farhood, A. & Jaeschke, H. Peroxynitrite is a critical mediator of acetaminophen hepatotoxicity in murine livers: Protection by glutathione. *J. Pharmacol. Exp. Ther.* **303**, 468–475 (2002).
20. Rahman, T. M. & Hodgson, H. J. Animal models of acute hepatic failure. *Int. J. Exp. Pathol.* **81**, 145–157 (2000).
21. Fan, F. et al. Pharmacological targeting of kinases MST1 and MST2 augments tissue repair and regeneration. *Sci. Transl. Med.* **8**, 352ra108–352ra108 (2016).
22. Chen, S. et al. Hepatocyte-specific Mas activation enhances lipophagy and fatty acid oxidation to protect against acetaminophen-induced hepatotoxicity in mice. *J. Hepatol.* **78**, 543–557 (2023).
23. Ben-Moshe, S. et al. The spatiotemporal program of zonal liver regeneration following acute injury. *Cell Stem Cell* **29**, 973–989 e910 (2022).
24. Dichamp, J. et al. In vitro to in vivo acetaminophen hepatotoxicity extrapolation using classical schemes, pharmacodynamic models and a multiscale spatial-temporal liver twin. *Front. Bioeng. Biotechnol.* **11**, 1049564 (2023).
25. Arnold, K. et al. Design of anti-inflammatory heparan sulfate to protect against acetaminophen-induced acute liver failure. *Sci. Transl. Med.* **12**, eaav8075 (2020).
26. Li, L. et al. SPHK1 deficiency protects mice from acetaminophen-induced ER stress and mitochondrial permeability transition. *Cell Death Differ.* **27**, 1924–1937 (2020).
27. Kolodziejczyk, A. A. et al. Acute liver failure is regulated by MYC- and microbiome-dependent programs. *Nat. Med.* **26**, 1899–1911 (2020).
28. Ezhilarasan, D. Molecular mechanisms in thioacetamide-induced acute and chronic liver injury models. *Environ. Toxicol. Pharmacol.* **99**, 104093 (2023).
29. Patel, S. J. et al. Gap junction inhibition prevents drug-induced liver toxicity and fulminant hepatic failure. *Nat. Biotechnol.* **30**, 179–183 (2012).
30. Li, Z. et al. Inhibition of TWEAK/Tnfrsf12a axis protects against acute liver failure by suppressing RIPK1-dependent apoptosis. *Cell Death Discov.* **8**, 328 (2022).
31. Arvelo, M. B. et al. A20 protects mice from D-galactosamine/lipopolysaccharide acute toxic lethal hepatitis. *Hepatology* **35**, 535–543 (2002).
32. Xu, Y. et al. Human endoderm stem cells reverse inflammation-related acute liver failure through cystatin SN-mediated inhibition of interferon signaling. *Cell Res.* **33**, 147–164 (2023).
33. Huang, S. et al. Lupeol ameliorates LPS/D-GalN induced acute hepatic damage by suppressing inflammation and oxidative stress through TGFβ1-Nrf2 signal pathway. *Aging* **13**, 6592–6605 (2021).
34. Zhu, Y. Z., Wu, W., Zhu, Q. & Liu, X. Discovery of Leonuri and therapeutical applications: From bench to bedside. *Pharmacol. Ther.* **188**, 26–35 (2018).
35. Li, Y. Y. et al. Leonurine: From gynecologic medicine to pleiotropic agent. *Chin. J. Integr. Med.* **26**, 152–160 (2020).
36. Ning, K. et al. eNOS-Nitric Oxide system contributes to a novel antiatherogenic effect of leonurine via inflammation inhibition and plaque stabilization. *J. Pharmacol. Exp. Ther.* **373**, 463–475 (2020).
37. Woolbright, B. L. & Jaeschke, H. The impact of sterile inflammation in acute liver injury. *J. Clin. Transl. Res.* **3**, 170–188 (2017).
38. Ni, H. M., Bockus, A., Boggess, N., Jaeschke, H. & Ding, W. X. Activation of autophagy protects against acetaminophen-induced hepatotoxicity. *Hepatology* **55**, 222–232 (2012).
39. Begriche, K., Massart, J., Robin, M. A., Borgne-Sanchez, A. & Fromenty, B. Drug-induced toxicity on mitochondria and lipid metabolism: mechanistic diversity and deleterious consequences for the liver. *J. Hepatol.* **54**, 773–794 (2011).
40. Hajovsky, H. et al. Metabolism and toxicity of thioacetamide and thioacetamide S-oxide in rat hepatocytes. *Chem. Res. Toxicol.* **25**, 1955–1963 (2012).
41. Story, D. L., Gee, S. J., Tyson, C. A. & Gould, D. H. Response of isolated hepatocytes to organic and inorganic cytotoxins. *J. Toxicol. Environ. Health* **11**, 483–501 (1983).
42. Kheradpezhouh, E., Ma, L., Morphett, A., Barritt, G. J. & Rychkov, G. Y. TRPM2 channels mediate acetaminophen-induced liver damage. *Proc. Natl. Acad. Sci. USA* **111**, 3176–3181 (2014).
43. Roy, S. et al. miR-1224 inhibits cell proliferation in acute liver failure by targeting the antiapoptotic gene Nfib. *J. Hepatol.* **67**, 966–978 (2017).
44. Yamauchi, T. et al. Cloning of adiponectin receptors that mediate antidiabetic metabolic effects. *Nature* **423**, 762–769 (2003).
45. Bretscher, A., Reczek, D. & Berryman, M. Ezrin: A protein requiring conformational activation to link microfilaments to the plasma membrane in the assembly of cell surface structures. *J. Cell Sci.* **110**, 3011–3018 (1997).
46. Wiche, G. Role of plectin in cytoskeleton organization and dynamics. *J. Cell Sci.* **111**, 2477–2486 (1998).
47. Li, B., Wu, J. & Li, X. Simultaneous determination and pharmacokinetic study of stachydrine and leonurine in rat plasma after oral administration of Herba Leonuri extract by LC-MS/MS. *J. Pharm. Biomed. Anal.* **76**, 192–199 (2013).
48. Suguro, R. et al. Anti-hypercholesterolemic effects and a good safety profile of SCM-198 in animals: From ApoE knockout mice to rhesus monkeys. *Front. Pharmacol.* **9**, 1468 (2018).
49. Zhang, Z. et al. The stabilization effect of dielectric constant and acidic amino acids on arginine-arginine (Arg-Arg) pairings: database survey and computational studies. *J. Phys. Chem. B* **117**, 4827–4835 (2013).
50. Hon, W. M., Lee, K. H. & Khoo, H. E. Nitric oxide in liver diseases: friend, foe, or just passerby? *Ann. N. Y. Acad. Sci.* **962**, 275–295 (2002).
51. Taylor, B. S., Alarcon, L. H. & Billiar, T. R. Inducible nitric oxide synthase in the liver: regulation and function. *Biochemistry* **63**, 766–781 (1998).
52. Marino, F. et al. Physical exercise and cardiac repair: The potential role of nitric oxide in boosting stem cell regenerative biology. *Antioxidants* **10**, https://doi.org/10.3390/antiox10071002 (2021).
53. Rai, R. M. et al. Impaired liver regeneration in inducible nitric oxide synthasedeficient mice. *Proc. Natl. Acad. Sci. USA* **95**, 13829–13834 (1998).
54. Carnovale, C. E. & Ronco, M. T. Role of nitric oxide in liver regeneration. *Ann. Hepatol.* **11**, 636–647 (2012).
55. Mount, P. F., Kemp, B. E. & Power, D. A. Regulation of endothelial and myocardial NO synthesis by multi-site eNOS phosphorylation. *J. Mol. Cell Cardiol.* **42**, 271–279 (2007).
56. Cai, H., Liu, D. & Garcia, J. G. CaM Kinase II-dependent pathophysiological signalling in endothelial cells. *Cardiovasc. Res.* **77**, 30–34 (2008).
57. Radi, R. Oxygen radicals, nitric oxide, and peroxynitrite: Redox pathways in molecular medicine. *Proc. Natl. Acad. Sci. USA* **115**, 5839–5848 (2018).

58. Gu, Q. et al. Genetic ablation of solute carrier family 7a3a leads to hepatic steatosis in zebrafish during fasting. *Hepatology* **60**, 1929–1941 (2014).
59. Garcia-Villafranca, J., Guillen, A. & Castro, J. Involvement of nitric oxide/cyclic GMP signaling pathway in the regulation of fatty acid metabolism in rat hepatocytes. *Biochem. Pharmacol.* **65**, 807–812 (2003).
60. Chen, H., Montagnani, M., Funahashi, T., Shimomura, I. & Quon, M. J. Adiponectin stimulates production of nitric oxide in vascular endothelial cells. *J. Biol. Chem.* **278**, 45021–45026 (2003).
61. Liao, L. et al. Leonurine ameliorates oxidative stress and insufficient angiogenesis by regulating the PI3K/Akt-eNOS signaling pathway in H2O2-induced HUVECs. *Oxid. Med. Cell. Longev.* **2021**, 9919466 (2021).
62. Alderton, W. K., Cooper, C. E. & Knowles, R. G. Nitric oxide synthases: structure, function and inhibition. *Biochem. J.* **357**, 593–615 (2001).
63. Aoyagi, M., Arvai, A. S., Tainer, J. A. & Getzoff, E. D. Structural basis for endothelial nitric oxide synthase binding to calmodulin. *EMBO J.* **22**, 766–775 (2003).
64. Schneider-Poetsch, T. et al. Inhibition of eukaryotic translation elongation by cycloheximide and lactimidomycin. *Nat. Chem. Biol.* **6**, 209–217 (2010).
65. Tanabe, H. et al. Human adiponectin receptor AdipoR1 assumes closed and open structures. *Commun. Biol.* **3**, 446 (2020).
66. Vasiliauskaite-Brooks, I. et al. Structural insights into adiponectin receptors suggest ceramidase activity. *Nature* **544**, 120–123 (2017).
67. Iwabu, M. et al. Adiponectin and AdipoR1 regulate PGC-1alpha and mitochondria by Ca(2+) and AMPK/SIRT1. *Nature* **464**, 1313–1319 (2010).
68. Broutier, L. et al. Human primary liver cancer-derived organoid cultures for disease modeling and drug screening. *Nat. Med.* **23**, 1424–1435 (2017).
69. Huch, M. et al. In vitro expansion of single Lgr5+ liver stem cells induced by Wnt-driven regeneration. *Nature* **494**, 247–250 (2013).
70. Huch, M. et al. Long-term culture of genome-stable bipotent stem cells from adult human liver. *Cell* **160**, 299–312 (2015).
71. Ouchi, R. et al. Modeling steatohepatitis in humans with pluripotent stem cell-derived organoids. *Cell Metab.* **30**, 374–384 (2019).
72. Kruitwagen, H. S. et al. Long-term adult feline liver organoid cultures for disease modeling of hepatic steatosis. *Stem Cell Rep.* **8**, 822–830 (2017).
73. Zhang, C. J. et al. A human liver organoid screening platform for DILI risk prediction. *J. Hepatol.* **78**, 998–1006 (2023).
74. Davies, N. A. & Banares, R. A new horizon for liver support in acute liver failure. *J. Hepatol.* **63**, 303–305 (2015).
75. Walesky, C. M. et al. Functional compensation precedes recovery of tissue mass following acute liver injury. *Nat. Commun.* **11**, 5785 (2020).
76. Riordan, S. M. & Williams, R. Acute liver failure: targeted artificial and hepatocyte-based support of liver regeneration and reversal of multiorgan failure. *J. Hepatol.* **32**, 63–76 (2000).
77. Ruart, M. et al. Impaired endothelial autophagy promotes liver fibrosis by aggravating the oxidative stress response during acute liver injury. *J. Hepatol.* **70**, 458–469 (2019).
78. Starkey Lewis, P. et al. Alternatively activated macrophages promote resolution of necrosis following acute liver injury. *J. Hepatol.* **73**, 349–360 (2020).
79. Bianchi, M. E. et al. High-mobility group box 1 protein orchestrates responses to tissue damage via inflammation, innate and adaptive immunity, and tissue repair. *Immunol. Rev.* **280**, 74–82 (2017).
80. Craig, D. G. et al. Staggered overdose pattern and delay to hospital presentation are associated with adverse outcomes following paracetamol-induced hepatotoxicity. *Br. J. Clin. Pharmacol.* **73**, 285–294 (2012).
81. Yang, R., Miki, K., He, X., Killeen, M. E. & Fink, M. P. Prolonged treatment with N-acetylcystine delays liver recovery from acetaminophen hepatotoxicity. *Crit. Care* **13**, R55 (2009).
82. Bernal, W. et al. Lessons from look-back in acute liver failure? A single centre experience of 3300 patients. *J. Hepatol.* **59**, 74–80 (2013).
83. Yuan, X. et al. Preclinical efficacy and safety of encapsulated proliferating human hepatocyte organoids in treating liver failure. *Cell Stem Cell* **31**, 484–498 (2024).
84. Meacham, C. E. et al. Adiponectin receptors sustain haematopoietic stem cells throughout adulthood by protecting them from inflammation. *Nat. Cell Biol.* **24**, 697–707 (2022).
85. Harrison, S. A. et al. A phase 3, rndomized, controlled trial of resmetirom in NASH with liver fibrosis. *N Engl. J. Med.* **390**, 497–509 (2024).
86. Okada-Iwabu, M. et al. A small-molecule AdipoR agonist for type 2 diabetes and short life in obesity. *Nature* **503**, 493–499 (2013).
87. Sun, G. et al. Discovery of AdipoRon analogues as novel AMPK activators without inhibiting mitochondrial complex I. *Eur. J. Med. Chem.* **200**, 112466 (2020).
88. Yu, Y. et al. Leonurine alleviates acetaminophen-induced acute liver injury by regulating the PI3K/AKT signaling pathway in mice. *Int. Immunopharmacol.* **120**, 110375 (2023).
89. Chen, S., Zhou, Y., Chen, Y. & Gu, J. fastp: an ultra-fast all-in-one FASTQ preprocessor. *Bioinformatics* **34**, i884–i890 (2018).
90. Kim, D., Paggi, J. M., Park, C., Bennett, C. & Salzberg, S. L. Graph-based genome alignment and genotyping with HISAT2 and HISAT-genotype. *Nat. Biotechnol.* **37**, 907–915 (2019).
91. Anders, S., Pyl, P. T. & Huber, W. HTSeq-a Python framework to work with high-throughput sequencing data. *Bioinformatics* **31**, 166–169 (2015).
92. Robinson, M. D., McCarthy, D. J. & Smyth, G. K. edgeR: a Bioconductor package for differential expression analysis of digital gene expression data. *Bioinformatics* **26**, 139–140 (2010).
93. Charni-Natan, M. & Goldstein, I. Protocol for primary mouse hepatocyte isolation. *STAR Protoc.* **1**, 100086 (2020).


## Acknowledgements

We thank Xiuxia Gao and Chun Li at the SPR Core Facility of ShanghaiTech University for their technical support in SPR analysis. We thank Dr. Fubin Wang for the technical support in the procurement of ADIPOR2 recombinant proteins. This work was supported by the National Key R&D Program of China 2020YFA0803604 (G.L.), 2021YFA0805000 (G.L.) and the National Natural Science Foundation of China 82070636 (Zhirong W), 31970778, 32370887 (G.L.).

## Author contributions

G.L., Zhirong W, and L. C. supervised the project. R.W. labeled the probes and performed affinity purification and LC/MS. R.W., Y.C., J.H., B.M., Huikang Y., Zhe W., B.S., Huiran.Y., J.Z., H.L., and Q.L. performed cell and animal experiments and acquired the data. Y.C. and Huikang Y. performed the human liver organoid experiment. J.H. and Y.H. cloned the DNA constructs. Y.C. analyzed the RNA-seq data. Y.G. and Zhe W. assisted with the measurement of enzymatic activity. G.L., R.W., and Y.C. wrote the manuscript.

## Competing interests

The first author Rui Wang is the applicant and one of the inventors (Rui Wang, Yuguo Wang, Jienina Yu) of a patent (No. ZL202010091483.6) related to findings shown in Fig. 1. The patent has been authorized and covers the utilization of SCM-198 in preventing acute liver injury and promoting hepatic tissue repair and regeneration. This patent concerns only the first author, and the rest of the authors have no competing interests to declare.

## Additional information

**Supplementary information** The online version contains supplementary material available at https://doi.org/10.1038/s41467-024-55295-7.

**Correspondence** and requests for materials should be addressed to Liming Cheng, Zhirong Wang or Gufa Lin.

**Peer review information** *Nature Communications* thanks Souleiman EL BALKHI, Yuanyan Liu, and the other anonymous reviewer(s) for their contribution to the peer review of this work. A peer review file is available.